ABSTRACT

Title of Thesis:	DEVELOPMENT AND IN-SILICO EVALUATION OF A CLOSED-LOOP FLUID RESUSCITATION CONTROL ALGORITHM WITH MEAN ARTERIAL PRESSURE FEEDBACK
	Mohammad Alsalti, Master of Science, 2020
Thesis directed by:	Associate Professor Jin-Oh Hahn Department of Mechanical Engineering

In this thesis, a model-based closed-loop fluid resuscitation controller using mean arterial pressure (MAP) feedback is designed and later evaluated on an in-silico testbed. The controller is based on a subject specific model of blood volume and MAP response to fluid infusion. This simple hemodynamic model is described using five parameters only. The model was able to reproduce blood volume and blood pressure response to fluid infusion using an experimental dataset collected from 23 sheep and is therefore suitable to use for control design purposes. A model-reference adaptive control scheme was chosen to account for inter-subject variability captured in the parametric uncertainties of the underlying physiological model. Three versions of the control algorithm were studied under different measurement availability scenarios. In-silico evaluation of the three controllers was done using a comprehensive cardiovascular physiology model on a cohort of 100 virtually generated patients. Results clearly show that a tradeoff exists between tracking and estimation performance depending on measurement availability.

DEVELOPMENT AND IN-SILICO EVALUATION OF A CLOSED-LOOP FLUID RESUSCITATION CONTROL ALGORITHM WITH MEAN ARTERIAL PRESSURE FEEDBACK

by

Mohammad Salahaldeen Ahmad Alsalti

Thesis submitted to the Faculty of the Graduate School of the
University of Maryland, College Park, in partial fulfillment
of the requirements for the degree of
Master of Science
2020

Advisory Committee:
Associate Professor Jin-Oh Hahn, Chair/Advisor
Associate Professor Nikhil Chopra
Assistant Professor Axel Krieger

Acknowledgements

First, I would like to thank my family for their continuous support during my education. Without their help, I would not have been able to reach this point. For that I am most thankful.

Second, special thanks go to my advisor, Professor Hahn, without whom this work would not exist. His advice and close monitoring of my progress were essential in my development as a future researcher. I sincerely appreciate the time and effort he put in helping me complete my thesis. I hope that my work in this thesis can contribute in some small way to the amazing work he is leading. His dedication was inspirational and a great motivation to pursue a career in academia.

Sincere thanks to my thesis committee, Professor Chopra and Professor Krieger, for taking the time out of their busy schedule to go over my work. Their guidance is essential in shaping this thesis into a meaningful research work.

Also, I would like to thank my colleagues at the laboratory for control and information systems, especially Dr. Xin Jin and Ali Tivay. Their work formed the basis on top of which I built my thesis material, and their support during my stay here was fundamental to the completion of this work. Special thanks to my close friends at UMD: Sally, Roohollah, Victor and Lydia, for making this journey so memorable.

Finally, I would like to thank my sponsors, the Fulbright program through the US Department of state and AMIDEAST, for their support financially, administratively and educationally. This experience was a once in a lifetime opportunity and they helped make it come true.

Table of Contents

List of Tables

List of Figures

List of Abbreviations

ANGSHC   Angiotensin Renal Function Curve Shift Constant

ANGVMC   Angiotensin Multiplier Constant

ANOVA   Analysis of Variance

BV   Blood Volume

CAC   Composite Adaptive Control

CO   Cardiac Output

CV   Capacitance Venous Tree

HCT   Hematocrit

Hgb   Hemoglobin

HIL   Hardware In the Loop

HR   Heart Rate

HS   Heart Strength

ICF   Intracellular Fluid

ICG   Indocyanine Green Dye

ISF   Interstitial Fluid

IVF   Intravascular Fluid

LSE   Least Squares Estimator

LVEDV   Left Ventricular End Diastolic Volume

MAP   Mean Arterial Pressure

MDAPE   Median Absolute Performance Error

MDPE   Median Performance Error

MRAC   Model Reference Adaptive Control

MRC   Model Reference Control

NN   Fluid Filtration from Capillaries into Tissue Space Multiplier

NRMSE   Normalized Root Mean Square Error

PE   Performance Error

PID	Proportional Integral Derivative
RAB	Right Atrial Basic Resistance
RBC	Red Blood Cells
SV	Stroke Volume
SYMKID	Effects of Sympathetic Signals on Kidney Function Multiplier
SYSID	System Identification
TPR	Total Peripheral Resistance
UO	Urinary Output
VR	Venous Return
VVOB	Baseline Unstressed Venous Volume

Chapter 1: Introduction

1.1 Fluid Resuscitation

Fluid resuscitation is the process of replenishing bodily fluids lost by vomiting, diarrhea, hemorrhage, burn injuries or during combat. If not treated rapidly, the patient experience hypovolemic shock [1]–[5]. Currently, clinicians perform fluid resuscitation through titration of fluids like crystalloids, colloids, normal saline and blood plasma while monitoring one or more physiologic endpoints (blood pressure, urinary output, cardiac output…etc.) [6]. This process is time consuming and is susceptible to human errors such as not providing optimal infusion dose or inadequate resuscitation. Delayed fluid resuscitation was shown to be a major cause of increased mortality and morbidity [7] while in other cases, excess administration of fluids results in edema and lack of oxygen delivery to tissues [8]. Moreover, inter-subject variability as well as how severely hypovolemic a patient is calls for continuous monitoring of patients' hemodynamics while undergoing fluid resuscitation to effectively perform titration and admission of fluids with the least amount of fluid [9]. Therefore, it is desired to automate fluid resuscitation to help increase the quality of care and reduce the workload of clinicians.

1.2 Autonomous Fluid Resuscitation and Current Physiological Mathematical Models

The goal of an autonomous fluid resuscitation system is similar to the current clinical resuscitation procedure: infusing fluid until a physiologic endpoint restores to a target value set by the clinician. Attempts to develop and evaluate such systems are

not common. Most existing closed-loop resuscitation controllers are built on decision trees and gain tuning [10]–[13]. Realizing that there is much room for improving the efficacy and robustness of such systems, we ought to make use of credible mathematical models that can reproduce hemodynamic responses to fluid infusion for controller design. The design of a model-based controller for a physiological phenomenon is as complex as the underlying mathematical model. Therefore, a simple yet accurate model is sought to allow for relatively simple design procedures.

Mathematical models that can reproduce hemodynamic responses to blood volume perturbations do exist. However, they suffer from one, or more, of the following disadvantages: (i) they are very complex involving hard nonlinearities and large number of parameters, which makes the design process of a model-based controller very difficult [14]–[19], or (ii) they are described using average values over a population, which no longer makes the model an individualized one that can capture intersubject variability [20], [21], and finally (iii) a class of these models are "black-box" models that do not offer deep physiological interpretation [22]–[25].

Recently, a control-theoretic model of blood volume response to fluid infusion was shown to be able to reproduce results from experimental data [26]. This model captures the fluid shift between the intravascular and interstitial blood compartments, a primary mechanism in hemostasis. Described using four parameters only, this model is simple, accurate and can be used for model-based controller design very efficiently. Since absolute blood volume is not easily measured even in a lab setting, we propose an extension to the blood volume model to include mean arterial pressure response to fluid infusion by means of a time varying gain that describes the relationship between blood

2

pressure and blood volume perturbations. This model was able to reproduce blood volume and blood pressure perturbations to fluid infusion in a set of experimental data collected from 23 sheep. Now, we have a simple, five-parameter model with physiological plausibility that enables the design of a closed-loop fluid resuscitation controller with mean arterial pressure as therapeutic endpoint using design approaches that are well established in the field of control theory [27]–[30]. Such controllers can be easier to implement clinically since blood pressure measurements are easily obtained and good approximation of mean arterial pressure (MAP) is calculated using [31]

$$MAP = P_{dia} + \frac{1}{3}\left[P_{sys} - P_{dia}\right] \tag{1}$$

1.3 Controller Design Methodology and Evaluation

There are many sources of uncertainty when dealing with physiological systems, most importantly the inter-subject variability in both BV and MAP dynamics [32], [33]. Therefore, the choice of adaptive control theory was made to account for inter-subject variability that presents itself as uncertainty in the parameters of the underlying physiological model [27].

The extended model was used to design a closed-loop fluid resuscitation control algorithm that operates in two steps: (i) the hemodynamic model is individualized using the measurements collected from an initial fluid bolus infusion via system identification and (ii) a model reference adaptive controller (MRAC) is built using the model just individualized. This two-step control architecture was chosen to address persistent excitation condition in online parameter estimation.

3

Three different versions of the proposed controller are investigated under different measurement availability scenarios. To assess the performance of the three versions, rigorous tests were done on an in-silico testbed using a well-known model of human cardiovascular physiology developed by Arthur Guyton [34]. The tests were done on a cohort of 100 subjects that were virtually generated by randomly perturbing key parameters in Guyton's model within a plausible range. Results were statistically analyzed to examine the performance of the control algorithm in an in-silico scenario.

1.4 Goals and Outline

In this thesis, an adaptive model-based closed-loop fluid resuscitation control algorithm is designed and tested, in the goal of achieving an autonomous fluid resuscitation system. The underlying physiological model used for controller design is an extension to an existing blood volume response to fluid infusion and hemorrhage model. The model is first investigated from a physiological standpoint, then examined for its ability to reproduce hemodynamic responses using experimental data from 23 sheep. Later, a two-step control architecture using blood pressure feedback was later designed and tested on an in-silico testbed using a well-established model of human cardiovascular physiology on a cohort of 100 virtually generated patients. Finally, the tracking and estimation performance of the controller was evaluated under different measurement availability scenarios.

The thesis is organized as follows. In chapter 2, we cover the details of the physiological model used for control design and its validation with experimental data. In chapter 3, we present the design procedure of the control algorithm and analyze its

stability properties. In chapter 4, we present the in-silico testing procedure of the proposed controllers. In chapter 5, we present the results of this study and investigate them from a statistical standpoint and finally conclude this work by summarizing the main results and outlining future work.

Chapter 2: Blood Volume-Blood Pressure Response to Fluid Infusion

In this chapter, we will present the structure of the physiological model that describes blood volume and mean arterial pressure response to fluid infusion and hemorrhage. We begin by giving a brief physiological background on the key mechanisms relating blood volume and mean arterial pressure changes to fluid infusion. Then, we describe the structure of the mathematical model in two parts: (i) blood volume response to fluid infusion and (ii) blood pressure response to blood volume perturbations. Finally, we examine the model's validity by its ability to reproduce experimental data collected from 23 sheep.

2.1 Physiological Background: Fluid Shift Mechanism

Perturbations in blood volume are caused by fluid infusion or hemorrhage (fluid loss). Bodily fluids are distributed between two main compartments: intracellular and extracellular [31], [35]. As the names suggest, intracellular fluid exists within the cell body while extracellular fluid exists outside the cells (figure 1). Extracellular fluid is further split into two compartments: interstitial fluid, which is the fluid between the cells in the tissue, and intravascular fluid which is the blood and plasma that flow in the arteries and veins. When fluid is gained or lost, fluid shifts between these compartments to maintain hemostasis. The shift mechanism and net fluid shift are determined by the permeability of vessels, the hydrostatic and oncotic pressure gradients.
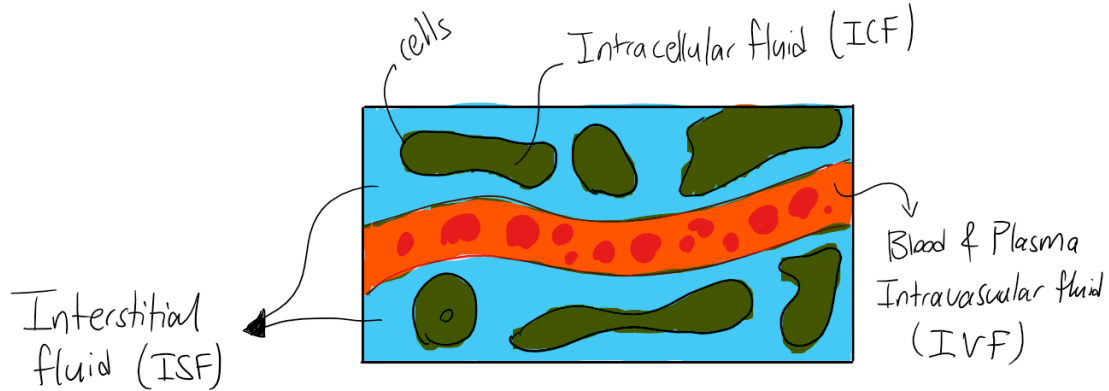
Figure 1: Body fluids compartments

Fluid shift occurs naturally depending on the body's state. For example, during burn injury fluid shifts from intravascular to interstitial fluid to compensate for fluids lost in affected tissues. This causes intravascular fluid to decrease, lowering blood volume and blood pressure. Low blood volume can lead to hypovolemia which is treated with fluid infusion (fluid resuscitation) using isotonic fluids such as crystalloids or colloids [4]. Similarly, excessive fluid shift from intravascular to interstitial compartment can lead to hypervolemia or edema. This is treated using diuretics that decrease blood volume and cause fluid to shift back to intravascular compartment from interstitial one [36].

2.2 Modeling of Blood Volume Response to Fluid Infusion and Hemorrhage

Given the complexity of the fluid shift mechanism, it is not easy to represent it mathematically in individual subjects. Current mathematical models that reproduce intravascular and interstitial volume changes in response to fluid infusion or loss are either black box models that lack physiological transparency and interpretability, or physiology-based first principle models that are complex and described by a large number of parameters. For such models, average values for parameters that are hard to

measure or estimate individually are used, which then makes the model not individualized but population-based [14]–[25].

Recent work [26] presents a lumped-parameter model that is described using only four parameters, physiologically plausible and can be individualized for each subject. This model leverages the physiological principle that fluid shift between intravascular and interstitial compartments, can be regarded as the output of a hypothetical feedback controller (figure 2). The net fluid gain (or loss) act on the blood volume compartment to alter the blood volume which in turn alters the interstitial fluid volume. The complex physiological processes that cause the fluid shift are summarized by the two-way valve action. The valve action determines the amount of fluid flow between the two compartments $q(t)$ based the discrepancy between the target $r_B(t)$ versus actual blood volume change $\Delta V_B(t)$. The objective of the controller is to regulate the volume changes in intravascular and interstitial compartments at a target ratio of $1{:}\alpha$ by retaining $1/(1+\alpha)$ fraction of the infused fluid in the intravascular compartment and shifting $\alpha/(1+\alpha)$ to the interstitial compartment.

Infused fluids usually consist of electrolytes (crystalloids) such as Lactated Ringer's solution or starch (colloids) such as Hextend, while lost fluids are usually plasma and red blood cells. Due to the difference in composition between infused and lost fluids, we denote the ratio between intravascular and interstitial volumetric changes in the steady state as α_u in the case of fluid gain (infusion) and α_v in the case of fluid loss (hemorrhage and urine). The block diagram of the model is shown in figure (3).

8
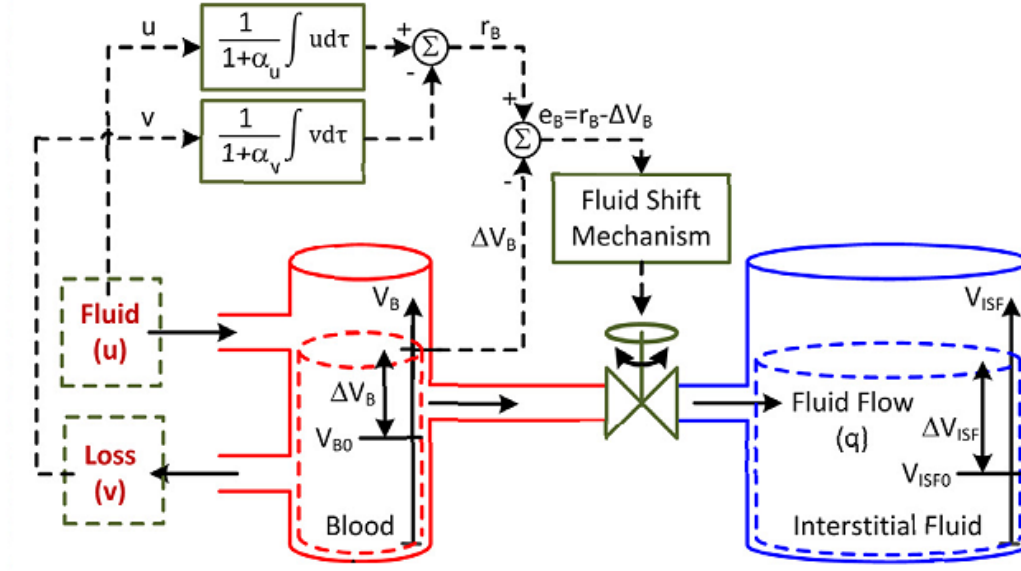
Figure 2: Control-theoretic blood volume response to fluid infusion model
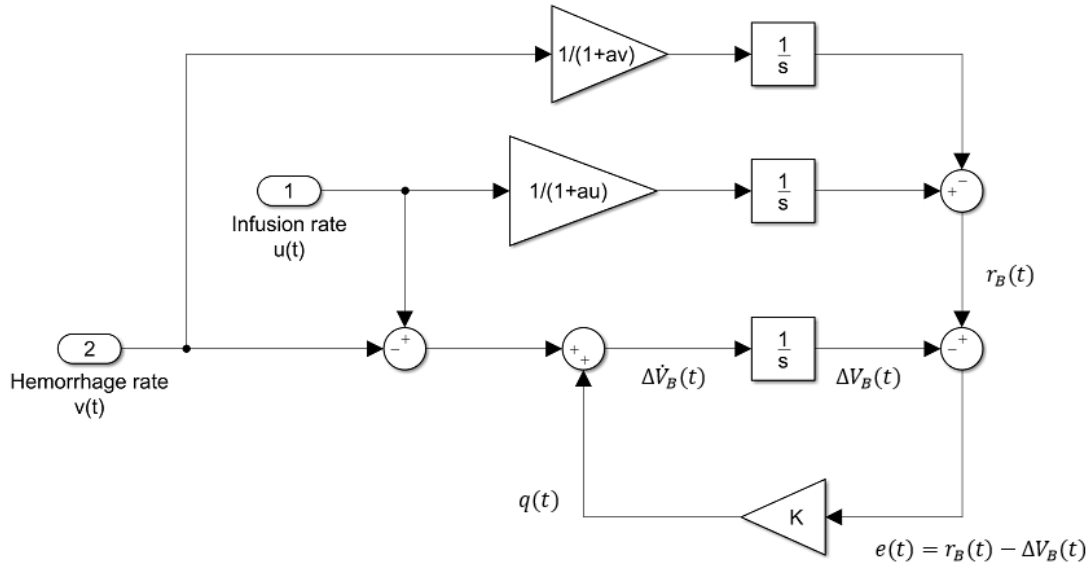
Figure 3: Block diagram of blood volume response to fluid infusion model

The desired steady-state change in BV $r_B(t)$, is written as

$$r_B(t) = \frac{1}{1+\alpha_u}\int_0^t u(\tau)d\tau + \frac{1}{1+\alpha_v}\int_0^t v(\tau)d\tau \qquad (2)$$

where $u(t)$ is the rate of fluid infusion and $v(t)$ is the rate of fluid loss due to

hemorrhage and urine. The inter-compartmental fluid shift is abstracted into the action

9

of a simple P-controller as a function of the discrepancy between the desired and actual changes in BV:

$$q(t) = q(e_B(t)) = K(r_B(t) - \Delta V_B(t)) \qquad (3)$$

where K is the feedback gain specifying the speed of fluid shift. Finally, by conservation of volume in the intravascular compartment we find that the rate of change in $\Delta V_B(t)$ is given by:

$$\Delta \dot{V}_B(t) = u(t) - v(t) - q(t) \qquad (4)$$

Combining equations (2)-(4) gives the complete differential equation describing blood volume changes in response to infusion and hemorrhage:

$$\Delta \ddot{V}_B(t) + K\Delta \dot{V}_B(t) = \dot{u}(t) - \dot{v}(t) + K\left(\frac{1}{1+\alpha_u}u(t) - \frac{1}{1+\alpha_v}v(t)\right) \qquad (5)$$

2.3 Modeling of Blood Pressure Response to Blood Volume Perturbations

Perturbations in blood volume (BV) caused by fluid shift entail perturbations in stroke volume and cardiac output. Stroke volume (SV) is the amount of blood pumped by the left ventricle per heartbeat while cardiac output (CO) is the amount of blood pumped by the left ventricle per minute [37]. These two can be related through:

$$CO(t) = SV(t) * HR(t) \qquad (6)$$

Moreover, venous return (VR) is defined as the amount of blood that returns to the right atrium per minute, which should be equal to cardiac output at steady state [31]. The effects of BV on SV and MAP are described from two complementary standpoints: (i) Arthur Guyton and his proposed cardiac output-venous return theory that relates changes in SV and CO, and hence BV, to blood pressure (specifically mean arterial

10

pressure MAP) through the total resistance of the veins and arteries (total peripheral resistance or TPR) [38] using the following equation:

$$CO(t) = \frac{MAP(t)}{TPR(t)} \tag{7}$$

From equation (7) we can express mean arterial pressure as:

$$MAP(t) = CO(t) * TPR(t) = SV(t) * HR(t) * TPR(t) \tag{8}$$

Arterial elastance (E_a) is defined as the product of heart rate and total peripheral resistance [31], [39]. Equation (8) then becomes:

$$MAP(t) = E_a(t) * SV(t) \tag{9}$$

(ii) The Frank-Starling mechanism with the left-ventricle pressure-volume loop theory dictates that changes in BV result in changes in SV and CO by altering the left ventricle end diastolic volume (LVEDV). This is described graphically in figure (4).
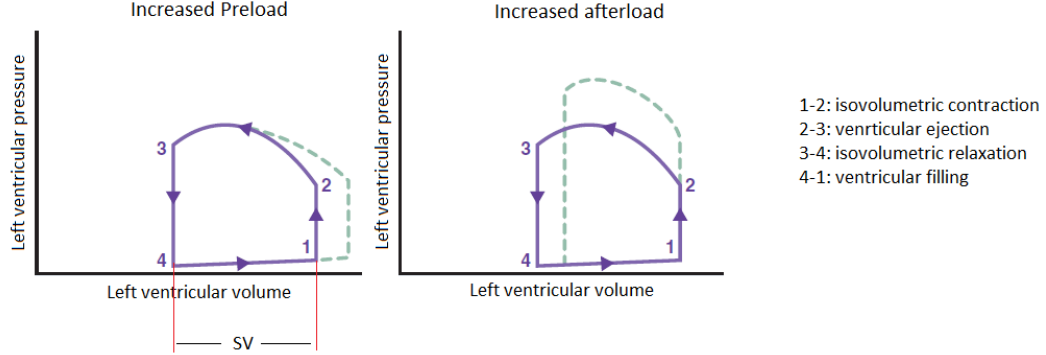
Figure 4: Left-ventricular pressure-volume curve. Increased preload causes an increase in stroke volume, while increased afterload causes a decrease in stroke volume.

Available data ([40], and figure(5)) suggests that a relationship exists between changes in stroke volume and changes in left ventricle volume, which in turn are affected by changes in blood volume. We propose to model this relationship between changes in SV and BV as:

11

$$\Delta SV(t) = K_{SV}(t)\Delta V_B(t) \tag{10}$$

where K_{SV} describes the sensitivity of SV to changes in BV.
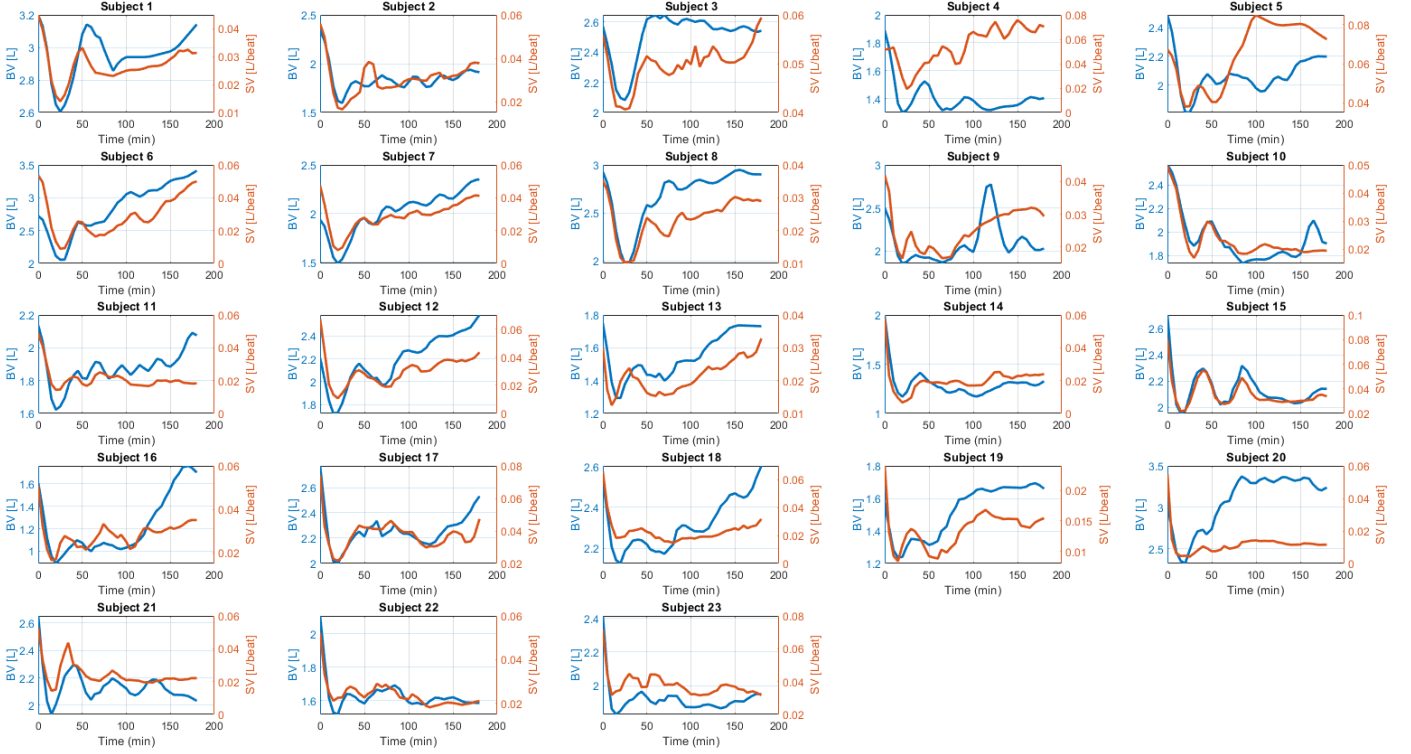
Figure 5: Sheep data shows a direct relationship between SV and BV

Using equations (9-10), we can write:

$$MAP(t) - MAP(0) = \Delta MAP(t) = E_a(t)SV(t) - E_a(0)SV_0$$

$$\Delta MAP(t) = (\Delta SV(t) + SV_0)E_a(t) - SV_0 E_a(0)$$

$$\Delta MAP(t) = \Delta SV(t)E_a(t) + SV_0 E_a(t) - SV_0 E_a(0)$$

$$\Delta MAP(t) = K_{SV}(t)\Delta V_B(t)E_a(t) + SV_0\Delta E_a(t) \tag{11}$$

$$\Delta MAP(t) = K_{SV}(t)E_a(t)\Delta V_B(t) + SV_0\frac{\Delta E_a(t)}{\Delta V_B(t)}\Delta V_B(t)$$

$$\Delta MAP(t) = \left[K_{SV}(t)E_a(t) + SV_0 K_{E_a}(t)\right]\Delta V_B(t)$$

where K_{E_a} is the sensitivity of changes in arterial elastance $E_a(t)$ to changes in blood volume (see figure (6)).
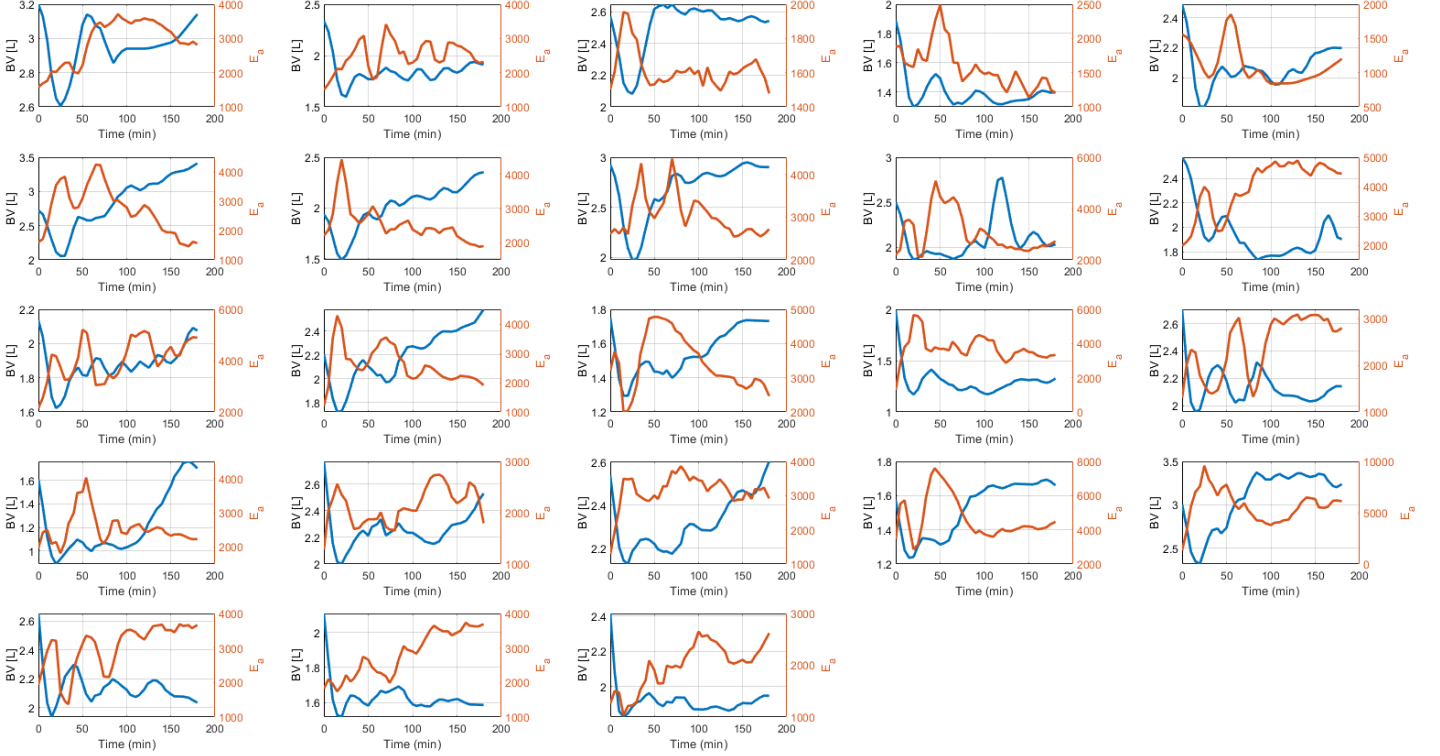
Figure 6: Sheep data shows opposite relationship between Ea and BV

The relationship between MAP and BV is now simply expressed as:

$$\Delta MAP(t) = K_{map}(t)\Delta V_B(t) \tag{12}$$

where $K_{map}(t) = K_{SV}(t)E_a(t) + SV_0 K_{E_a}(t)$ is a time-varying gain that captures the relationship between changes in MAP and BV. Finally, the full mathematical model describing blood pressure response to fluid perturbations can be described using the following differential equation

$$\frac{d^2}{dt}\big(\Delta MAP(t)\big) + K\frac{d}{dt}\big(\Delta MAP(t)\big) = K_{map}(t)\left\{[\dot{u}(t) - \dot{v}(t)] + K\left(\frac{1}{1+\alpha_u}u(t) - \frac{1}{1+\alpha_v}v(t)\right)\right\} \tag{13}$$

In the previous two sections, we provided the structure of the mathematical model of blood volume and blood pressure response to fluid infusion and hemorrhage. In this section, we validate the efficacy of this simple model and its ability to reproduce a set of experimental data collected from 23 sheep animals. Although model validation was done using sheep data, great similarities exist between human and sheep cardiovascular system which allow for control design for fluid infusion to human subjects. This section shows that a simple model with four parameters that can reproduce experimental data, is a valid choice for model-based control design.

2.4.1 Experimental Data

The experimental data were collected from 23 sheep undergoing controlled intravenous blood volume perturbations caused by hemorrhage and fluid infusion. Measurements included rates of infusion and hemorrhage, urinary output (UO), blood volume (BV), cardiac output (CO), blood pressure (mean arterial pressure MAP) and heart rate (HR). The protocol followed in conducting the experiment was approved by the Institutional Animal Care and Use Committee (IACUC) at the University of Texas Medical Branch [40]. The duration of study for each animal was 180 min. After recording baseline data, initial hemorrhage of 25 mL/kg was performed over 15 minutes. Fluid infusion was initiated 30 min after the start of the hemorrhage and continued for 150 minutes. Second and third hemorrhage of 5 mL/kg were performed 50 and 70 min after the start of the initial hemorrhage respectively, and each continued for 5 min. Fluid infusion was done with a rule-based closed-loop controller [41], [42].

Baseline BV (V_{B0}) was measured via indocyanine green dye (ICG) [43]. Moreover, Hematocrit (Hct), which is defined as the ratio between red blood cell volume and BV, was measured before and through the experiment at 5 to 10 min intervals. Hct measurements were used to calculate $V_B(t)$ for each subject as follows:

$$V_B(t) = \frac{V_{RBC}(t)}{Hct(t)}$$

$$\dot{V}_{RBC}(t) = -h(t)\frac{V_{RBC}(t)}{V_B(t)}$$

(14)

where $h(t)$ is the rate of fluid loss, $V_B(t) = \Delta V_B(t) + V_{B0}$ and $V_{RBC}(0) = Hct(0)V_{B0}$. Other hemodynamic responses were measured at same time instants.

2.4.2 System identification

A fully individualized system identification of the proposed hemodynamic model is performed. The model described by equation (13) is a time-varying linear model. Identification of time varying models is not a trivial task, in fact most literature that exists in this domain [44], [45] use a method of sliding time windows of certain width T and perform GLS (general least squares) then average the values over all time. Other methods include variations of Kalman filter where the time varying parameters are assumed to be driven by white noise [46]. We propose an alternative "two-layer" method for recursively estimating the model parameters (see figure (7)).
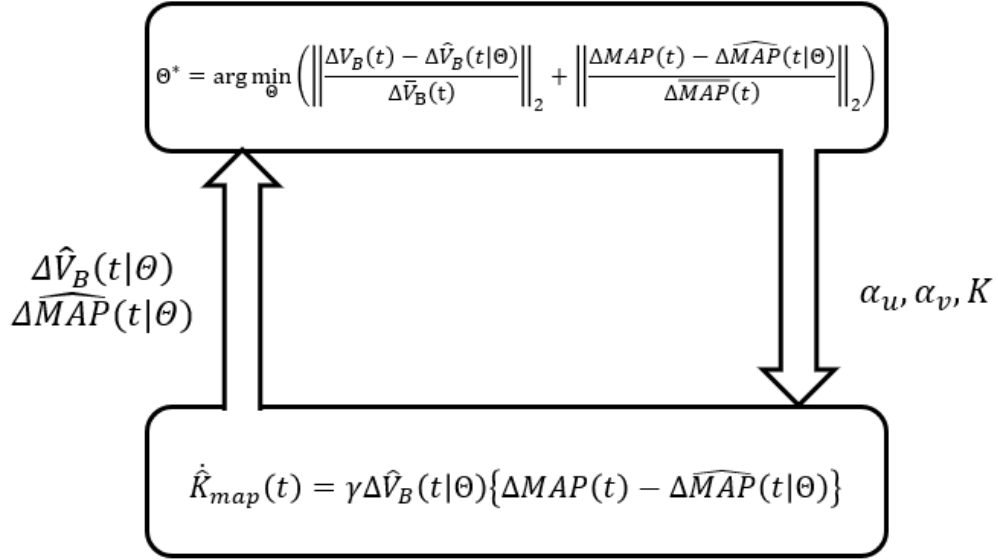
Figure 7: Two-level identification scheme for the hemodynamic linear time-varying model

The two-layer optimization problem was set up using MATLAB© (Natick, MA) optimization toolbox. In each loop of MATLAB's "fmincon" solver, a guess for BV model parameters (α_v, α_u, K) is given to solve for $\Delta \hat{V}_B(t)$. This drives a recursive least squares estimator that solves for $\hat{K}_{map}(t)$ using

$$\dot{\hat{K}}_{map}(t) = \gamma \Delta \hat{V}_B(t|\Theta)\{\Delta MAP(t) - \Delta \widehat{MAP}(t|\Theta)\} \tag{15}$$

From equation (15) we evaluate $\Delta \widehat{MAP}(t)$ as the product of $\hat{K}_{map}(t)$ and $\Delta \hat{V}_B(t)$. The optimization problem is solved for the optimal model parameters Θ^* by minimizing the discrepancy between predicted and actual measurements:

$$\Theta^* = \{\alpha_u^*, \alpha_v^*, K^*, K_{map}^*(t)\} = \arg\min_{\Theta} \left(\left\| \frac{\Delta V_B(t) - \Delta \hat{V}_B(t|\theta)}{\Delta \bar{V}_B(t)} \right\|_2 + \left\| \frac{\Delta MAP(t) - \Delta \widehat{MAP}(t|\theta)}{\Delta \overline{MAP}(t)} \right\|_2 \right) \tag{16}$$

Note that $\Delta V_B(t) = V_B(t) - V_{B0}$ and $\Delta MAP(t) = MAP(t) - MAP_0$ are the true values obtained from experimental data, $\Delta \bar{V}_B(t)$ and $\Delta \overline{MAP}(t)$ are the average values of the

true BV and MAP for all time respectively and finally, $\Delta \hat{V}_B(t|\Theta)$ and $\Delta \widehat{MAP}(t|\Theta)$ are the model predicted values at each time t and parameter estimates Θ.

2.4.3 Results

Results of the proposed system identification procedure are shown in figure (8) and table (1). Figure (8) shows the true vs model-predicted BV, MAP and $K_{map}(t)$ for sheep (2,4,7,10,12,21). True values of $K_{map}(t)$ were obtained by dividing $\Delta MAP / \Delta V_B$. We can see that the model was able to reproduce the experimental data to high accuracy in sheep (2,4,10,21). However, for some sheep (like 7, 12), we can see that lack of excitation of the recursive LSE (i.e: $\Delta \hat{V}_B(t) \approx 0$) caused inaccurate estimate for $K_{map}(t)$ and hence $\Delta MAP(t)$. One way to correct this is to increase the adaptation gain γ to higher values but risk fitting the noise in MAP data. Table (1) shows the results of model parameters $(\alpha_u^*, \alpha_v^*, K^*)$ for all 23 sheep as well as the RMSE for $K_{map}(t)$ estimation, MAP, and BV model predictions. When calculating RMSE for $K_{map}(t)$, numerical artifacts had to be taken care of when "true" $K_{map}(t)$ values goes to near infinite values.
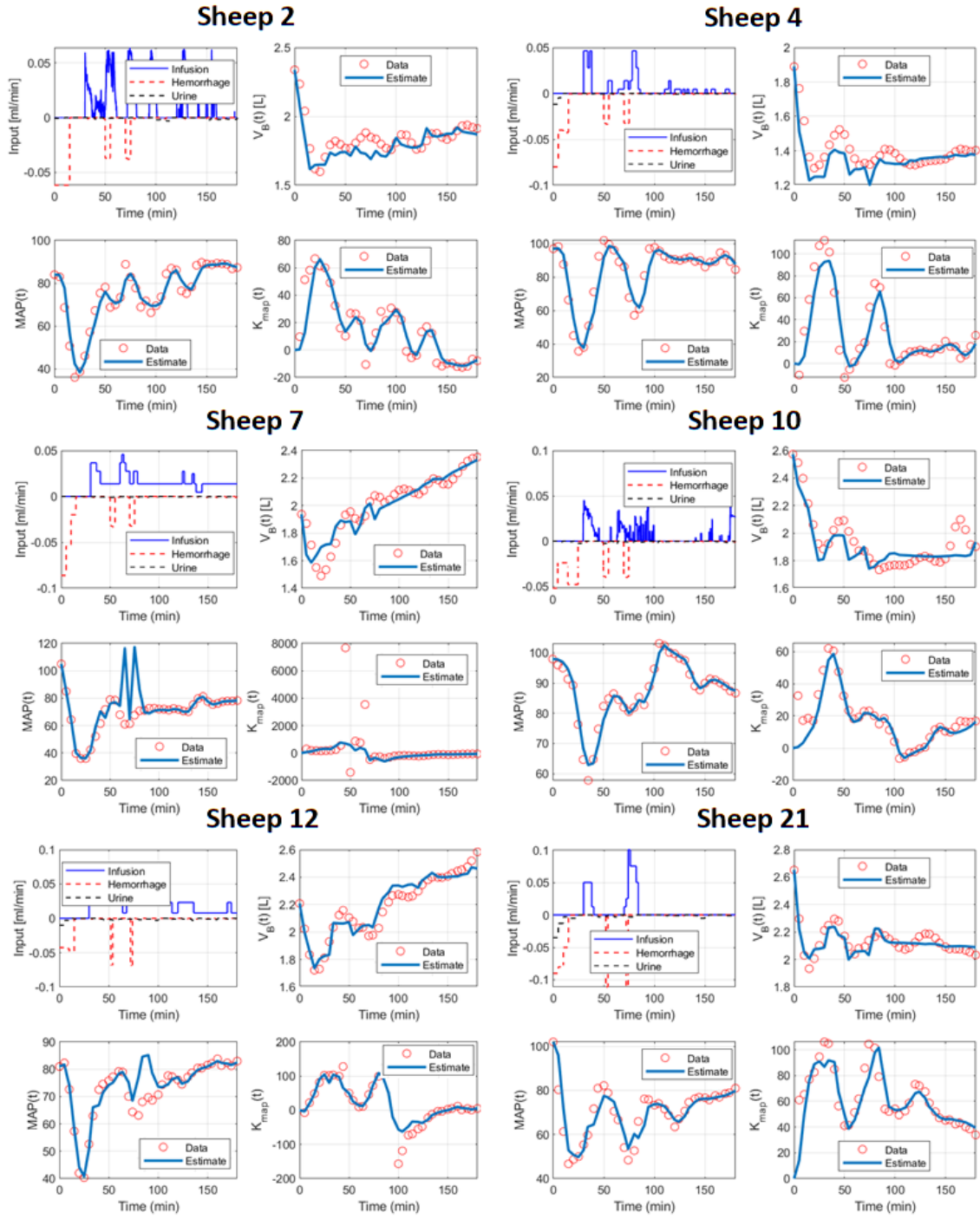
Figure 8: System identification results on sheep #2, 4, 7, 10, 12, 21

18

Table 1: System identification results

Sheep #	α_u	α_v	K	RMSE(K_{map}) [mmHg/L]	γ	RMSE($MAP(t)$) [mmHg]	RMSE($V_B(t)$) [L]
1	1.129371	0.736503	0.499937	6.425082	1	2.014615	0.064235
2	2.189056	0.350914	0.490442	0.267033	1	1.650505	0.035538
3	3.91598	2.999968	0.083817	1.6172	50	0.662869	0.060583
4	1.284306	0.405203	0.499873	0.403862	1	2.541623	0.037102
5	3.167091	0.78169	0.499951	0.830554	1	2.042132	0.033807
6	2.087496	1.277491	0.093277	6.0877	10	2.99855	0.03753
7	2.744221	2.798947	0.248002	16.3350	100	5.786654	0.038327
8	4.815708	0.92952	0.076127	5.9939	5	2.184243	0.06438
9	2.975871	0.949318	0.04115	1.302951	2	1.077198	0.091531
10	1.000036	0.319161	0.499991	0.584892	1	0.941307	0.044453
11	1.281386	1.192153	0.499917	3.400212	2	2.217937	0.032405
12	3.394052	1.027561	0.221095	2.3485	10	2.296417	0.028135
13	4.998773	1.075419	0.497458	3.6221	10	5.064654	0.036192
14	4.999959	0.113891	0.382841	0.447262	1	0.866377	0.061169
15	4.999802	0.755961	0.499986	0.413542	2	1.306922	0.033568
16	4.99991	0.435235	0.499956	13.49035	2	2.159152	0.069577
17	4.994477	1.067425	0.265812	0.416419	1	1.421104	0.041934
18	1.000029	2.332503	0.10981	4.236475	5	1.045553	0.033631
19	3.91019	2.36292	0.14011	1.454657	1000	1.84302	0.025485
20	2.144853	2.381776	0.152031	12.84891	1	4.483123	0.04187
21	4.314586	1.508877	0.343047	0.436498	1	2.373437	0.023738
22	3.470183	1.144868	0.499761	0.59534	1	2.317259	0.020845
23	1.745179	1.443239	0.447935	0.365676	1	1.863951	0.026929
mean	**3.111414**	**1.234371**	**0.330101**	**3.648875**		**2.224287**	**0.042738**
SD	**1.445251**	**0.797916**	**0.175089**	**4.666218**		**1.303912**	**0.017609**

Chapter 3: Development of Control Algorithm

In this chapter, we will highlight the control design steps and analyze its stability properties. We begin by explaining the motivation behind our choice of adaptive control methodology, followed by a set of assumptions to accommodate the application of adaptive control theory to the hemodynamic model described in chapter 2. Finally, details of the two-step control architecture are given, and its stability properties are analyzed.

3.1 Why adaptive control?

As shown in table (1), model parameters for 23 sheep are uncertain and lie within some range. This inter-subject (subject-to-subject) variability presented by parametric uncertainty in physiological models [32] can be addressed with the use of adaptive control theory. In adaptive control, an estimate of the uncertain plant parameters (or controller parameters) is obtained online from input-output data [27], [30], [47], [48]. These estimates are used in the control input to achieve a desired tracking performance despite the presence of disturbances, parameter uncertainty or unknown variations in plant parameters.

Although robust control design techniques also account for uncertainty, the choice of adaptive control over robust control lies in the learning behavior of adaptive control systems through online estimation, especially for systems with constant or slowly varying parameters. This gives superior performance since adaptive control systems improve performance as adaptation goes on, while robust controllers try to keep consistent performance over time. Moreover, adaptive control does not require a-priori

information in contrast to robust control which requires some knowledge of parameter bounds. The control design followed below is a modification of a semi-adaptive model reference adaptive control (MRAC) scheme, where the change in MAP follows a first order reference model trajectory.

3.2 Assumptions

To accommodate the application of control theory to the model described by equation (13), several assumptions must be made. First, the time-varying parameter $K_{map}(t)$ is assumed to be constant or slowly varying parameter $\left(K_{map}(t) \approx K_{map}\right)$. Second, in the resuscitation scenario described later in section (4.1), the hemorrhage (typically unknown) is assumed to have taken place and was stopped before the resuscitation process takes place. Therefore α_v and $v(t)$ will be omitted from equation (13). Moreover, the relationship between MAP and BV due to infusion is passive [49], which suggests that the sign of $K_{map}(t)$ is usually positive. That is, for patients that respond to fluid infusion by increasing blood volume, the result is an increase in blood pressure. If we consider the 23 sheep data from section (2.4), figure (9) clearly show that (K_{map}) is positive during the resuscitation phase for most subjects that responded to fluid infusion. Sheep #4,9 and 10 are example of such non-responsive subjects that did not effectively respond to fluid infusion.
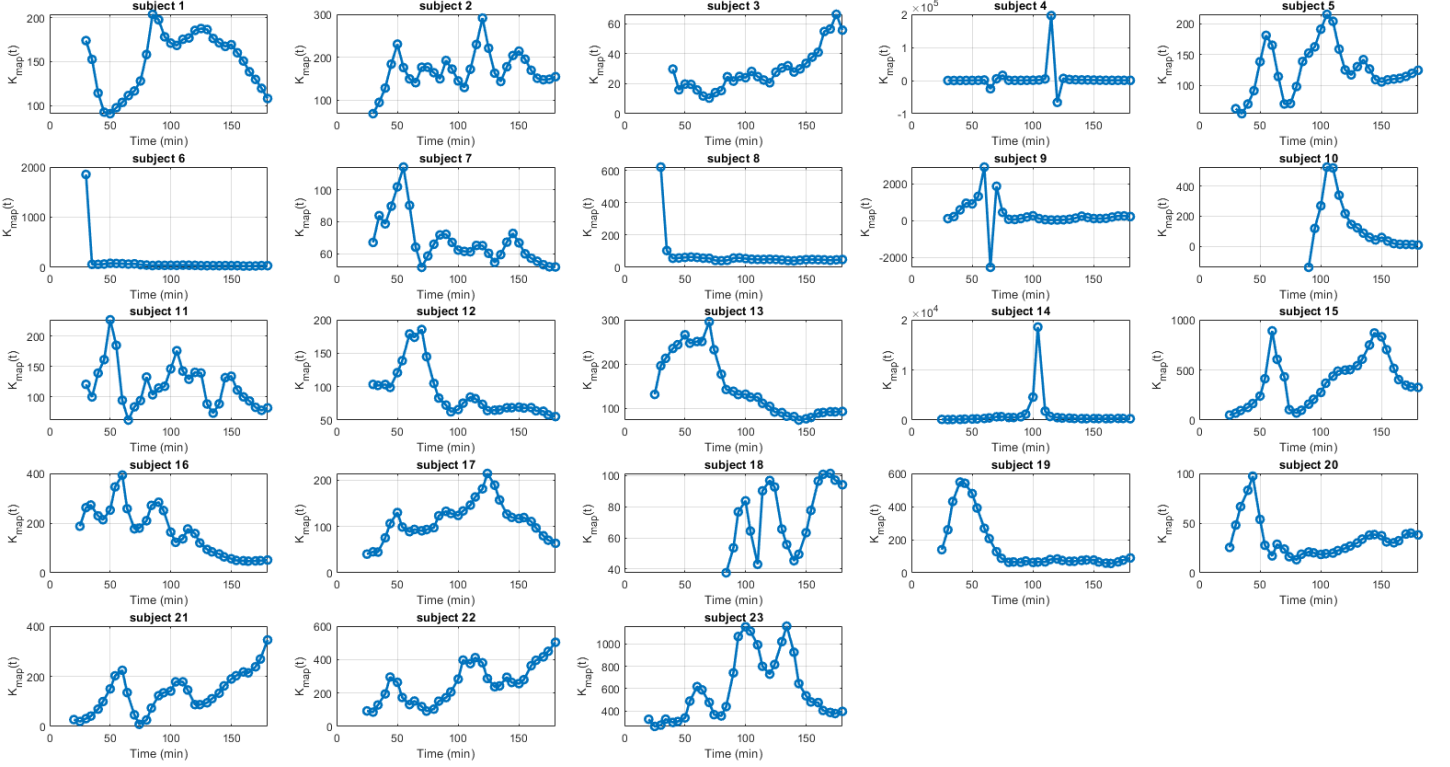
Figure 9: Sign (K_{map}) during fluid resuscitation

The mathematical model used for control design is now described by:

$$\frac{d^2}{dt}\big(\Delta MAP(t)\big) + K\frac{d}{dt}\big(\Delta MAP(t)\big) = K_{map}\left\{\dot{u}(t) + \frac{K}{1+\alpha}u(t)\right\} \qquad (17)$$

where α replaces α_u in equation (13). Equation (17) is a linear time-invariant version of equation (13) and can be represented by a transfer function of the form

$$G_p(s) = \frac{\Delta MAP(s)}{u(s)} = K_{map}\frac{s + \dfrac{K}{1+\alpha}}{s^2 + Ks} \qquad (18)$$

This plant transfer function meets all the assumptions (P1-P4) for MRAC control methodology [27] which are:

- P1: Transfer function numerator $Z_p(s)$ is a monic Hurwitz polynomial of degree m_p.

22

- P2: An upper bound n on the degree n_p of the transfer function denominator polynomial $R_p(s)$.

- P3: The relative degree $n^* = n_p - m_p$ of $G_p(s)$ is known.

- P4: The sign of the high frequency gain ($K_p = K_{map}$ in this case) is known.

3.3 Two-Step Control Architecture

Inspired by previous work [50], the patient is assumed to have suffered hemorrhage which has been stopped and treated. After that, the resuscitation algorithm is initiated and it operates in two steps: (i) an initial bolus infusion is administered to the patient and Hct and MAP measurements are recorded and used to estimate the hemodynamic model parameters in equation (17). (ii) a model-reference adaptive controller (MRAC) built on the individualized model regulates the blood pressure of the patient while estimating $K_{map}(t)$ online. Although an adaptive control algorithm should individualize the hemodynamic model and estimate its parameters on its own, safe fluid infusion profiles prevents the algorithm from fulfilling persistent excitation (rich input signals) conditions. The proposed two-step architecture is intended to overcome such challenges by providing an accurate estimate of the model parameters through batch system identification in step (1), for the online parameter estimator to initialize from. Moreover, this simulation scenario only involves resuscitation only (i.e.: not RBC are lost). This allows for the approximation of Hct measurements by the following equation [51], preserving the linearity of the system:

$$\frac{\Delta V_B(t)}{V_{B0}} = \frac{Hct(0) - Hct(t)}{Hct(t)} \tag{19}$$

23

Figure (10) below shows how the two-step architecture of the control algorithm in further detail.
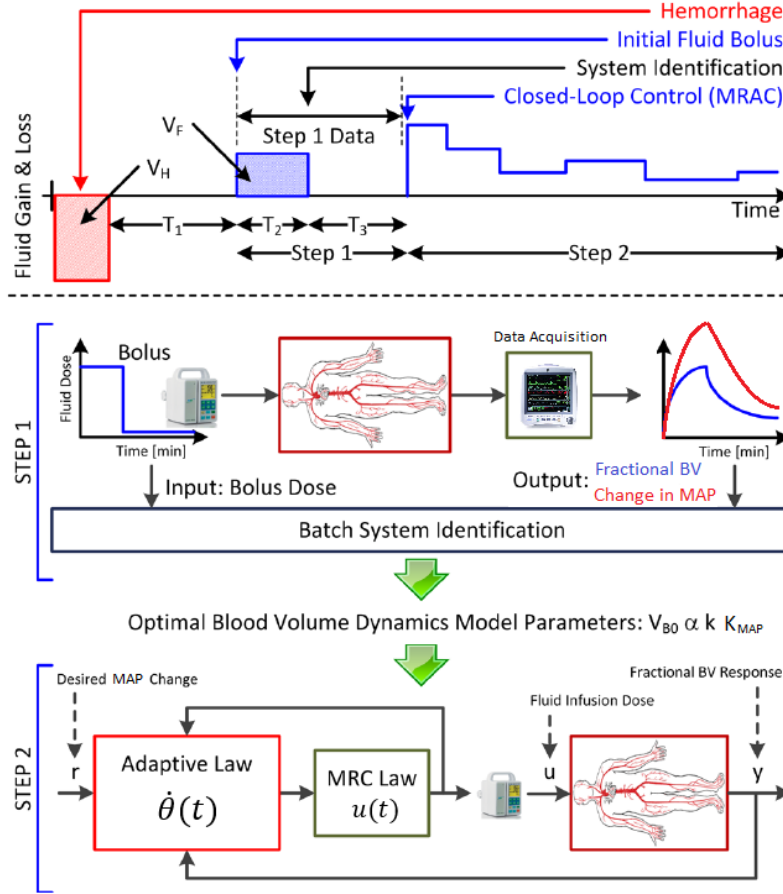

Figure 10: Two-step control architecture

3.3.1 Step (1): Batch System Identification

In step (1) described above, the patient receives a bolus infusion while the Hematocrit (equivalently $y_1(t) = \Delta V_B(t)/V_{B0}$ approximation) and MAP $(y_2(t))$ measurements are recorded for 40 min. For each patient, these measurements are used to estimate the model parameters using batch system identification techniques. To identify the model parameters, equation (17) is first discretized using forward Euler approximation for differentiation, which gives:

24

$$\Delta MAP(i+2) + (KT_s - 2)\Delta MAP(i+1) + (1 - KT_s)\Delta MAP(i)$$

$$= K_{map}T_s\, u(i+1) + \left[K_{map}KT_s^2 \frac{1}{1+\alpha_u} - K_{map}T_s\right]u(i) \tag{20}$$

where (i) is the discrete-time index and (T_s) is the sampling time. Optimal model parameters are then found by solving the following minimization problem

$$\Theta^* = \{\alpha^*, K^*, V_{B0}^*, K_{map}^*\} = \arg\min_\Theta(\omega_1\|y_1(i) - \hat{y}_1(i|\Theta)\|_2 + \omega_2\|y_2(i) - \hat{y}_2(i|\Theta)\|_2) \tag{21}$$

where $\hat{y}_1$ and $\hat{y}_2$ refer to the model predicted fractional blood volume change and MAP change. The optimal values $\{\alpha^*, K^*, V_{B0}^*, K_{map}^*\}$ minimize the weighted sum of norms of prediction errors in both y_1 and y_2. Note that, because of the approximation in (19), we require to estimate one more parameter in this setting (V_{B0}), which represents the blood volume prior to the beginning of infusion. However, if only MAP measurements were available, then we solve for the following minimization problem:

$$\Theta^* = \{\alpha^*, K^*, K_{map}^*\} = \arg\min_\Theta\|y_2(i) - \hat{y}_2(i|\Theta)\|_2 \tag{22}$$

3.3.2 Step (2): Model Reference Adaptive Control

A model-reference adaptive controller is constructed using the estimated model parameters $\{\alpha^*, K^*, V_{B0}^*, K_{map}^*\}$. MRAC structure decomposes into two components: (i) the model reference control law (MRC) obtained by model matching, and (ii) the update law. In the design of a model reference control law, the control input is designed to have $y_2(t) = \Delta MAP(t)$ track a desired reference trajectory described by a first order reference model, given by the following transfer function

$$W_m(s) = \frac{y_m(s)}{r(s)} = \frac{a_m}{s + a_m} \tag{23}$$

where y_m is the desired time evolution of $MAP(t)$, a_m is the model's time constant of 15 minutes and r is the reference target value of $\Delta MAP(t)$ (i.e.: the desired change in MAP from the first measurement). The goal of MRC is to achieve perfect tracking by asymptotically driving the output tracking error $e_{tr}(t) = y_2(t) - y_m(t)$ to zero. The reference model in equation (23) also meets the reference model assumptions [27] which are:

- M1: reference model transfer function numerator and denominator polynomials are monic Hurwitz polynomials of degree q_m, p_m respectively where $p_m \leq n$.

- M2: The relative degree $n_m^* = p_m - q_m$ of is the same as that for $G_p(s)$.

Now consider the following control law as shown in figure (11):

$$u(t) = \frac{\theta_1}{s + \lambda} u(t) + \frac{\theta_2}{s + \lambda} y_2(t) + \theta_3 y_2(t) + \theta_4 r(t) \qquad (24)$$
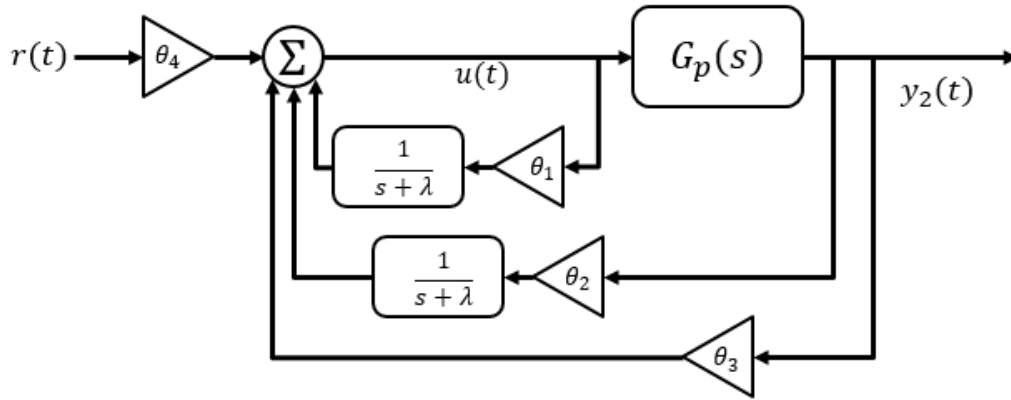

Figure 11: Model-Reference Control law [27]

where $\lambda > 0$. Substituting equation (24) in (18) gives the following closed-loop transfer function:

26

$$y_2(s) = \frac{\theta_4 K_{map}\left(s + \frac{K}{1+\alpha}\right)(s + \lambda)}{(s + \lambda - \theta_1)(s^2 + Ks) - K_{map}\left(s + \frac{K}{1+\alpha}\right)(\theta_2 + \theta_3(s + \lambda))} r(s) \qquad (25)$$

For perfect model matching, the transfer function in (25) must be equal to the reference

model transfer function (23). This is known as the certainty equivalence principle and

is used to find the mapping between plant parameters and controller parameters.

Equating the two transfer functions gives:

$$\frac{a_m}{s + a_m} = \frac{\theta_4 K_{map}\left(s + \frac{K}{1+\alpha}\right)(s + \lambda)}{(s + \lambda - \theta_1)(s^2 + Ks) - K_{map}\left(s + \frac{K}{1+\alpha}\right)(\theta_2 + \theta_3(s + \lambda))} \qquad (26)$$

Solving equation (26) for the controller parameters $\theta_1, \theta_2, \theta_3, \theta_4$ yields:

$$\theta_1 = \lambda - \frac{K}{1+\alpha} \qquad\qquad \theta_3 = \frac{[K - a_m - \lambda]}{K_{map}}$$

$$\qquad\qquad (27)$$

$$\theta_2 = \frac{[\lambda^2 - \lambda K]}{K_{map}} \qquad\qquad \theta_4 = \frac{a_m}{K_{map}}$$

and the control law (24) becomes:

$$u(t) = \left(\lambda - \frac{K}{1+\alpha}\right)\frac{u(t)}{s + \lambda} + \frac{1}{K_{map}}\left\{[\lambda^2 - \lambda K]\frac{y_2(t)}{s + \lambda} + [K - a_m - \lambda]y_2(t) + a_m r(t)\right\} \qquad (28)$$

However, true controller parameters θs are not known because true $\{\alpha, K, K_{map}\}$ are

unknown. Our best approximation to the control law so far is to replace the parameters

$\{\alpha, K, K_{map}\}$ with their batch system identification estimates $\{\alpha^*, K^*, K_{map}^*\}$ from

either (21) or (22), depending on available measurements. As described in chapter (2),

α and K are regarded as constant parameters and will be fixed at their batch system

identification result $\{\alpha^*, K^*\}$. An online parameter estimate can now be applied to

estimate $\theta = \dfrac{1}{K_{map}}$. True θ is replaced by its estimate $\theta(t)$ in the control law (28) to

yield:

$$u(t) = \left(\lambda - \frac{K^*}{1+\alpha^*}\right)\frac{u(t)}{s+\lambda} + \theta(t)\left\{[\lambda^2 - \lambda K^*]\frac{y_2(t)}{s+\lambda} + [K^* - a_m - \lambda]y_2(t) + a_m r(t)\right\} \quad (29)$$

The update law for $\theta(t)$ is derived using Lyapunov theory in the following section

3.4 Adaptive Law and Stability Analysis

We investigate the stability of the adaptive law proposed in section (3.3) using the

following Lyapunov analysis. The output y_2 in figure (10) can be expressed as [30]:

$$y_2(t) = y_m(t) + \frac{a_m}{s+a_m}\frac{K_{map}}{a_m}\tilde{\theta}(t)\left\{[\lambda^2 - \lambda K^*]\frac{y_2(t)}{s+\lambda} + [K^* - a_m - \lambda]y_2(t) + a_m r(t)\right\} \quad (30)$$

where $\tilde{\theta}(t) = \theta(t) - \theta$ denotes the parameter estimation error. Let the tracking error

be $e_{tr}(t) = y_2(t) - y_m(t)$ so that:

$$e_{tr}(t) = \frac{a_m}{s+a_m}\frac{K_{map}}{a_m}\tilde{\theta}(t)\left\{[\lambda^2 - \lambda K^*]\frac{y_2(t)}{s+\lambda} + [K^* - a_m - \lambda]y_2(t) + a_m r(t)\right\} \quad (31)$$

For notational simplicity, let

$$\psi(t) = \left\{[\lambda^2 - \lambda K^*]\frac{y_2(t)}{s+\lambda} + [K^* - a_m - \lambda]y_2(t) + a_m r(t)\right\} \quad (32)$$

For Lyapunov stability analysis we propose the following Lyapunov function

$$V\left(e_{tr}(t), \tilde{\theta}(t)\right) = \frac{1}{2}e_{tr}(t)^2 + \frac{1}{2\gamma}K_{map}\tilde{\theta}(t)^2 \quad (33)$$

The time derivative of (32) is given by:

$$\dot{V}\left(e_{tr}(t), \tilde{\theta}(t)\right) = e_{tr}(t)\dot{e}_{tr}(t) + \frac{1}{\gamma}K_{map}\tilde{\theta}(t)\dot{\tilde{\theta}}(t) \quad (34)$$

The derivative of the tracking error is obtained by re-arranging equation (31)

28

$$\dot{e}_{tr}(t) = -a_m e_{tr}(t) + K_{map}\tilde{\theta}(t)\psi(t) \tag{35}$$

Substituting (35) into equation (34) gives:

$$\dot{V}\left(e_{tr}(t), \tilde{\theta}(t)\right) = -a_m e_{tr}^2(t) + e_{tr}(t)K_{map}\tilde{\theta}(t)\psi(t) + \frac{1}{\gamma}K_{map}\tilde{\theta}(t)\dot{\tilde{\theta}}(t) \tag{36}$$

Since the assumption was made earlier that $K_{map}(t)$ is a constant or slowly varying parameter, then $\dot{\tilde{\theta}}(t) = \dot{\theta}(t)$. To ensure negative definiteness of the time derivative of Lyapunov function, we choose the adaptation law of $\theta(t)$ as

$$\dot{\theta}(t) = -\gamma e_{tr}(t)\left\{[\lambda^2 - \lambda K^*]\frac{y_2(t)}{s+\lambda} + [K^* - a_m - \lambda]y_2(t) + a_m r(t)\right\} \tag{37}$$

Plugging equation (37) back into (36) gives

$$\dot{V}\left(e_{tr}(t), \tilde{\theta}(t)\right) = -a_m e_{tr}^2(t) \leq 0 \tag{38}$$

Since $V(e_{tr}(t), \tilde{\theta}(t))$ is positive definite and $\dot{V}(e_{tr}(t), \tilde{\theta}(t))$ is negative semi-definite, then $V(e_{tr}(t), \tilde{\theta}(t))$ is bounded. Hence, the plant model (18) and the adaptation law (37) are globally stable and consequently, $e(t), \psi(t)$ and $\tilde{\theta}(t)$ are bounded. Since $e(t)$ and $\tilde{\theta}(t)$ are bounded, then $\dot{e}(t)$ is bounded as in (35). Moreover, since $\dot{V}(e_{tr}(t), \tilde{\theta}(t))$ is bounded, then $\ddot{V}(e_{tr}(t), \tilde{\theta}(t))$ is also bounded and by invoking Barbalat's lemma we find that $\dot{V}(e_{tr}(t), \tilde{\theta}(t))$ is uniformly continuous and $\lim_{t\to\infty} \dot{V} = \lim_{t\to\infty} e(t) = 0$. Therefore, stability of the proposed control algorithm is guaranteed.

To evaluate the controller performance under different measurement availability scenarios, we will introduce composite adaptation terms into equation (35). First, we will make use of both fractional blood volume measurements y_1 and MAP measurements y_2 in the adaptation law as a combination of tracking error $e_{tr}(t) = y_m(t) - y_2(t)$ and y_1-prediction error terms:

29

$$\dot\theta(t) = -\gamma_1 e_{tr}(t)\psi(t) + \gamma_2 \left[y_1(t) - \theta(t)\frac{y_2(t)}{V_{B0}^*} \right] \frac{y_2(t)}{V_{B0}^*} \tag{39}$$

The composite term in equation (39) is trying to minimize the input prediction error

between true y_1 and estimated $\hat{y}_1 = \frac{\Delta V_B}{V_{B0}^*} = \frac{y_2}{\hat{K}_{map}(t)V_{B0}^*} = \frac{\theta(t)y_2}{V_{B0}^*}$. We refer to equation

(39) as the 2-measurement composite adaptation scheme.

Similarly, we will consider using MAP measurements only, which is more clinically

plausible since fractional blood volume measurements are not easy to obtain. When

only MAP measurements are available, we use an adaptation law that is a combination

of tracking error $e_{tr}(t)$ and input-prediction error $(u(t) - \hat{u}(t))$ instead of y_1-

prediction error term. The composite term is derived by re-writing the plant's input in

terms of the controller parameters, and then use the gradient rule to minimize the input-

prediction error $e_{pr,u}$ [30].

$$y_2 = K_{map}\frac{\left(s + \dfrac{K^*}{1+\alpha^*}\right)}{s(s+K^*)}u$$

$$\frac{1}{K_{map}}\frac{s+K^*}{s+\dfrac{K^*}{1+\alpha^*}}y_2 = \frac{u}{s} \tag{40}$$

$$\theta(t)\frac{s+K^*}{s+\dfrac{K^*}{1+\alpha^*}}y_2 = \frac{u}{s}$$

Define the input-prediction error term as

$$e_{pr,u}(t) = \theta(t)\frac{s+K^*}{s+\dfrac{K^*}{1+\alpha^*}}y_2(t) - \frac{u(t)}{s} \tag{41}$$

30

$$\therefore \dot{\theta}(t) = -\gamma_2 \left[\frac{s + K^*}{s + \frac{K^*}{1 + \alpha^*}} y_2 \right] e_{pr,u} \tag{42}$$

We can now simply augment equation (37) with the composite term (equation 42) to get the following single-measurement composite adaptation scheme:

$$\dot{\theta}(t) = -\gamma_1 e_{tr}(t)\psi(t) - \gamma_2 \left[\frac{s + K^*}{s + \frac{K^*}{1 + \alpha^*}} y_2(t) \right] \left(\theta(t) \frac{s + K^*}{s + \frac{K^*}{1 + \alpha^*}} y_2(t) - \frac{u(t)}{s} \right) \tag{43}$$

where $\psi(t) = \left\{ [\lambda^2 - \lambda K^*] \frac{y_2(t)}{s+\lambda} + [K^* - a_m - \lambda] y_2(t) + a_m r(t) \right\}$.

To summarize, in this chapter we proposed a two-step control architecture to regulate MAP to a set-value following a reference model trajectory. In-silico simulation scenario assumes that a patient suffers hemorrhage which is then stopped and treated, after which a two-step resuscitation control algorithm is initiated. First step involves a bolus fluid infusion and measurement collection which are later used to individualize the underlying hemodynamic model. Then, a semi-adaptive model reference adaptive controller is built using the individualized model to regulate MAP to a set-value. The control law is given in equation (29), and is expressed as:

$$u(t) = \left(\lambda - \frac{K^*}{1 + \alpha^*} \right) \frac{u(t)}{s + \lambda} + \theta(t) \left\{ [\lambda^2 - \lambda K^*] \frac{y_2(t)}{s+\lambda} + [K^* - a_m - \lambda] y_2(t) + a_m r(t) \right\}$$

with the parameter $\theta(t)$ being the online estimate of $1/K_{map}$. To evaluate the performance of the controller and online estimation of $\theta(t)$ under different measurement availability scenarios, we proposed three versions for $\theta(t)$ update laws:

- Plain MRAC:

$$\dot{\theta}(t) = -\gamma e_{tr}(t)\psi(t)$$

31

- Single measurement composite adaption scheme:

$$\dot{\theta}(t) = -\gamma_1 e_{tr}(t)\psi(t) - \gamma_2 \left[\theta(t)\frac{s+K^*}{s+\frac{K^*}{1+\alpha^*}}y_2(t) - \frac{u(t)}{s}\right]\left(\frac{s+K^*}{s+\frac{K^*}{1+\alpha^*}}y_2(t)\right)$$

- 2-measurement composite adaptation scheme:

$$\dot{\theta}(t) = -\gamma_1 e_{tr}(t)\psi(t) + \gamma_2 \left[y_1(t) - \theta(t)\frac{y_2(t)}{V_{B0}^*}\right]\frac{y_2(t)}{V_{B0}^*}$$

where again, $\psi(t) = \left\{[\lambda^2 - \lambda K^*]\frac{y_2(t)}{s+\lambda} + [K^* - a_m - \lambda]y_2(t) + a_m r(t)\right\}$. In the next chapter, a rigorous in-silico evaluation of the proposed controller, with the corresponding three variations of the update law, is conducted using a highly nonlinear, well-known model of human cardiovascular physiology developed by Arthur Guyton [34].

Chapter 4: In-Silico Evaluation of Proposed Controllers

In this chapter, we will present a rigorous in-silico evaluation of the controllers discussed in chapter 3. First, we will explain the simulation resuscitation scenario, then we will show how the controllers perform on the same model used for control design (for proof of concept). For a more rigorous evaluation, we used a highly nonlinear, well established computer model of human cardiovascular physiology developed by Arthur Guyton [34] as basis for our in-silico testbed. Using this model, we generated a cohort of 100-virtual subjects by perturbing key model parameters within a physiological range. Results are analyzed and discussed in further detail in chapter 5.

4.1 In-silico Testing Scenario

The testing scenario is as follows: the patient is assumed to have lost blood (or fluid) prior to the resuscitation process, then after hemorrhage is treated and stopped, an initial bolus infusion is given followed by the closed loop control action (see figure (12)). For simulation purposes, the lost blood is assumed to be a total of 2.5L over a time period of 120 minutes. Then, 120 minutes after hemorrhage had taken place, we begin resuscitation by first infusing a fluid bolus of 0.5L for 30 minutes, then monitor the patient's response for 10 minutes. During these 40 minutes, the patient's fractional blood volume and mean arterial pressure data are collected and used in "step 1: batch system identification" (check section 3.3.1 above). Then, 160 minutes after the patient had experienced hemorrhage, the MRAC adaptive control law, built using the collected data, is initiated to regulate mean arterial blood pressure to some set-point given by the clinician (for simulation purposes, this set point is an increase of 30mmHg in MAP).
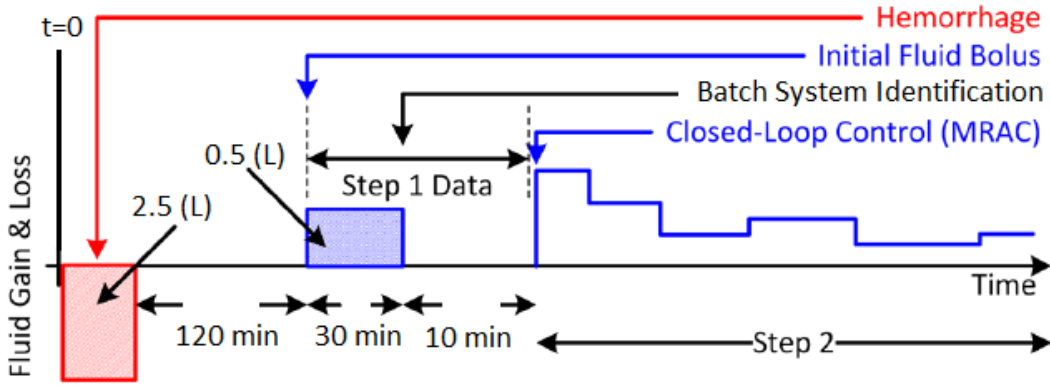
33

Figure 12: In-silico resuscitation scenario

4.2 Proof of Concept of Proposed Control Law

It is usually a good rule of thumb to test the controller on the same model used for controller design. Results are expected to be identical to what theory dictates in chapter 3, and the reason behind showing such results it to ensure that the controller works and help understand the controllers' performance when tested on a more realistic (highly nonlinear) model later in this chapter.

4.2.1 Plain MRAC and Single-Measurement Composite Adaptation Schemes

As explained in chapter 3, we investigated different versions of the controller's update law: (i) plain MRAC update law, (ii) single-measurement composite adaptation scheme and (iii) 2-measurement composite adaptation scheme. In this section we will show the results of testing the controller on the same simplified model used for controller design for the first two versions, i.e.: using plain MRAC and single-measurement composite adaptation. For sake of simulation, model parameters were chosen within a physiological range as $\alpha = 1.3478$, $V_{B0} = 4.6043$, $K = 0.0946$ and $K_{map} = 40$. The reason for investigating the two cases together is that both update laws

34

use MAP measurements only, and therefore share the same procedure for step (1) batch system identification that solves for model parameters using (22). As seen in figure (13), the estimated parameters perfectly match the model parameters.
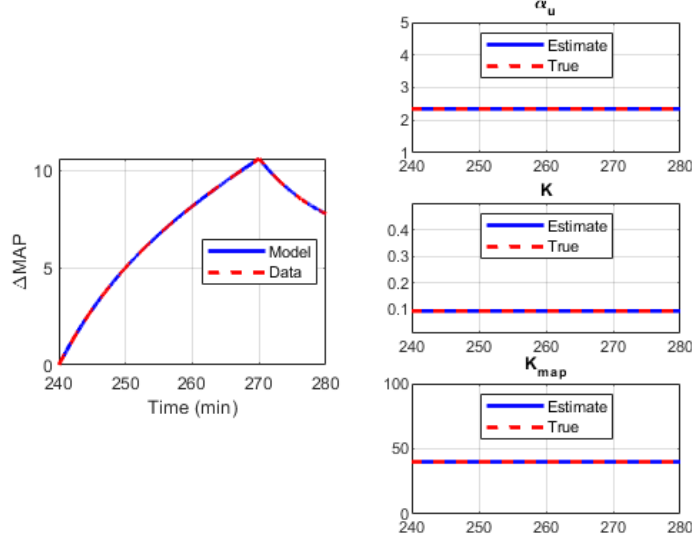
Figure 13: Batch system identification results for plain MRAC and single-measurements case

At this point the MRAC control law is initiated to regulate MAP to a set point of 30 mmHg increase along with the adaptive laws (equations 37 and 40 respectively) to estimate K_{map} online. The results of equation (37) shown in figure (14a) clearly show the effect of lack of information when using plain MRAC as opposed to using the single-measurement composite adaptation scheme in figure (14b) (equation 43). As reported in [52], the use of input-prediction error composite term in the adaptation rule clearly enhanced tracking performance as well as online estimation.
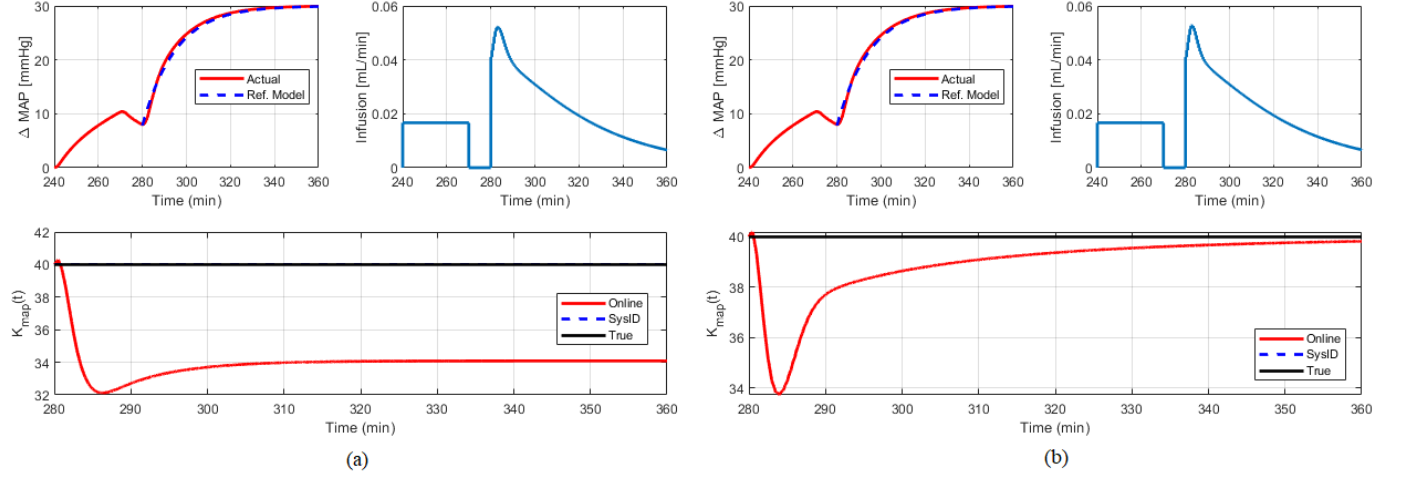
Figure 14: Tracking and online estimation performance for (a) plain MRAC and (b) single-measurement composite adaptation

4.2.2 Two-Measurements Composite Adaptation Scheme

Here we follow a similar procedure to the one followed in section 4.2.1, except that in the batch system identification step we use both measurements to solve for the model parameters $V_{B0}, \alpha, K,$ and K_{map} as in equation (21). Again, the estimated parameters perfectly match the model parameters as seen in figure (15). The tracking and estimation performance, as given by equations (29, 39), is shown in figure (16). It is clear from figure (16) that availability of both sources of information (namely, Hct and MAP) allowed us to achieve perfect tracking of $K_{map}(t)$ online without requiring a persistently exciting input.

36
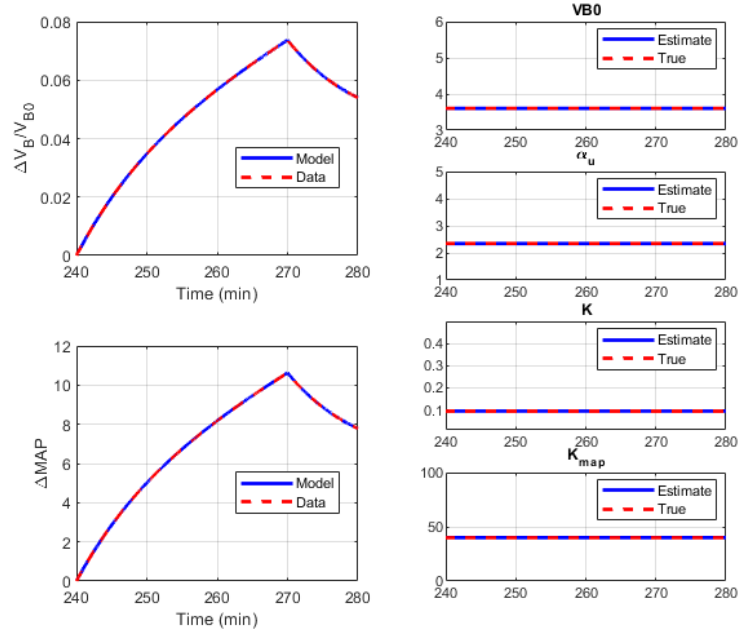
Figure 15: Batch system identification results for two-measurements case
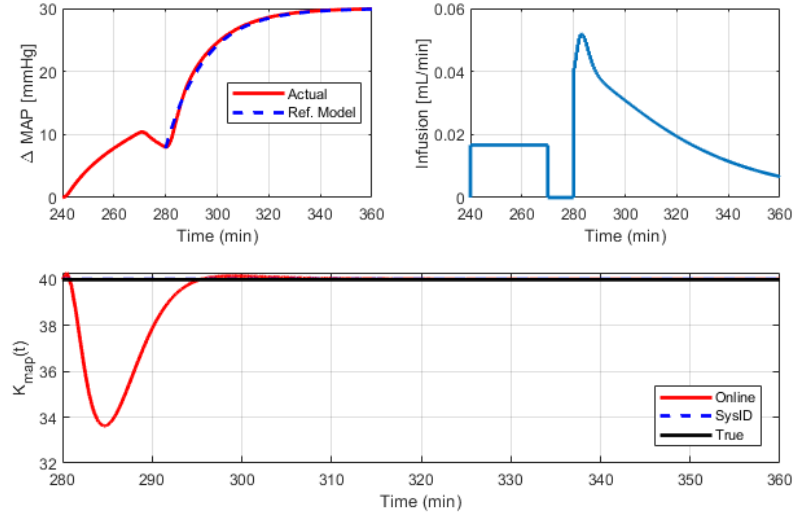
Figure 16: Tracking and online estimation performance in the presence of two measurements

4.3 Guyton's Model and Virtual Subjects Generation

Arthur Guyton in [34] developed a computer simulation model as an analysis

tool of the circulatory system designed specifically to study most of the important

37

factors that control arterial pressure. As seen in figure (17) the model is divided into eight sub-models: (1) circulatory dynamics, (2) interstitial fluid, (3) autoregulation, (4) sympathetic simulation, (5) kidney output, (6) pressure positive feedback, (7) function curve adaptation, and (8) angiotensin. Slight extensions were made to this model in order to accommodate the application of the proposed closed-loop fluid resuscitation control algorithm: (i) Introduce the capability of the model to simulate hemorrhage and resuscitation. Such blood volume changes were simulated by adding and subtracting fluid to the intravascular compartment directly. (ii) Incorporate plasma volume and red blood cells change that are required to calculate hematocrit Hct(t).
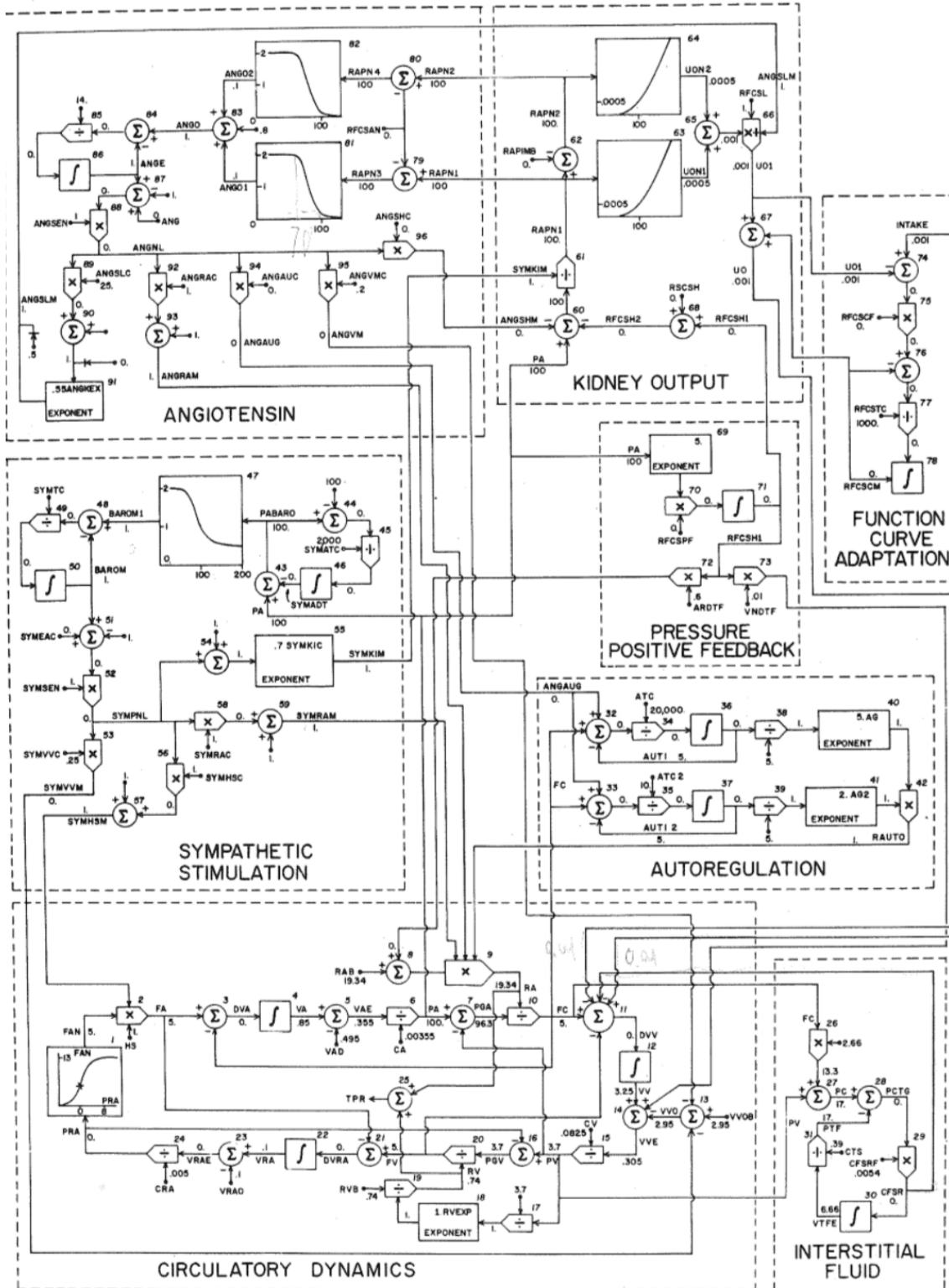
Figure 17: Guyton's computer simulation model of human circulatory system

The computer model proposed by Arthur Guyton has over 40 constant parameters describing the interactions between 8 intermediate subsystems that control the arterial pressure. Out of the 40 parameters, some are key "multiplier factors" which generally determine the physiology of the simulated patient. For example, Heart Strength (HS) represents the heart pumping capacity and is used to calculate cardiac output by multiplying it with sympathetic stimulation. Another example is Basic Arterial Resistance (RAB) which is used along with other signals to calculate TPR (total peripheral resistance) eventually. Table (2) summarizes the key parameters of Guyton's model

Table 2: Summary of Guyton's model key parameters

Parameter	Physiological Interpretation	Parameter	Physiological Interpretation
RAB	Baseline arterial resistance	SYMKID	Effects of sympathetic signals on kidney function multiplier
HS	Heart strength multiplier	ANGVMC	Angiotensin multiplier constant
NN	Fluid filtration from capillaries into tissue space multiplier	ANGSHC	Angiotensin renal function curve shift constant
CV	Capacitance venous tree	VVOB	Baseline unstressed venous volume

By randomly perturbing these key parameters from their nominal values within a plausible physiological range, we generated a cohort of 100 virtual subjects, which will be used to conduct the in-silico testing. Guyton's model is based on human physiology so it should be noted again that although we verified the proposed cardiovascular model using sheep data (section 2.4), the great similarities that exist between human and sheep cardiovascular physiology allow us to use our controller for human in-silico testing

40

scenarios. Figure (18) shows the samples that were drawn for the 100 virtual patients of the 8 key parameters. Also shown in figure (18) is the range of pre-hemorrhage blood volume [5-5.5 L] and mean arterial pressure [80-120 mmHg] for the 100 virtual subjects.
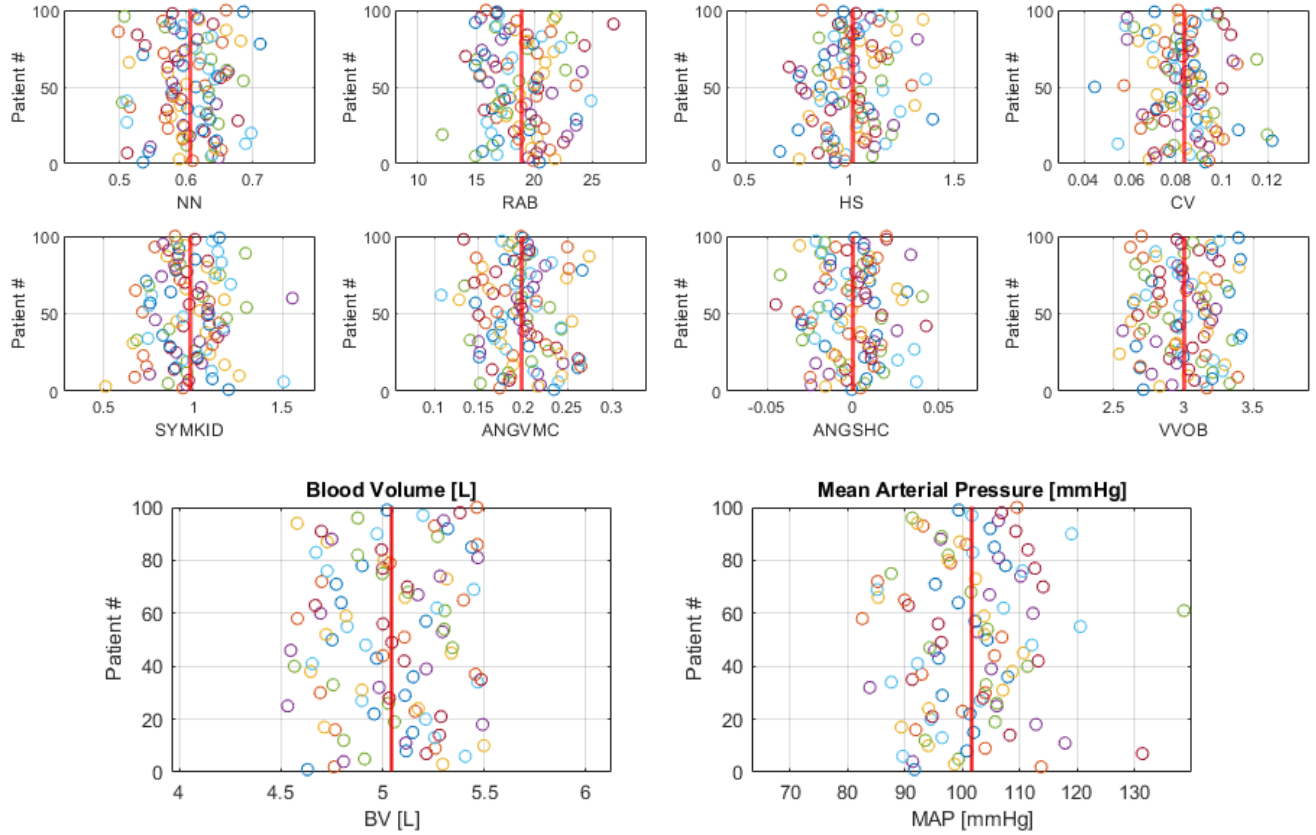

Figure 18: Model parameters distribution and BV-MAP values for all 100 subjects

To make the testing scenario as realistic as possible, the algorithm was implemented digitally with a sampling time of 0.5 min. Moreover, fractional blood volume and mean arterial pressure measurements were contaminated by adding a uniform random noise of sizable magnitude (+/- 0.01 and +/- 2 mmHg) respectively. This reflects the inaccuracy in blood hematocrit saturation and MAP measurements [53]. To dampen the effect of the measurement noise on the control algorithm, these measurements were

smoothed using 6-point moving average digital filter before being used in both steps of the control architecture.

4.4 Simulation Results

In this section, we will show simulation results on Guyton's model for a nominal subject (i.e: 5L pre-hemorrhage blood volume and 100mmHg pre-hemorrhage mean arterial pressure).
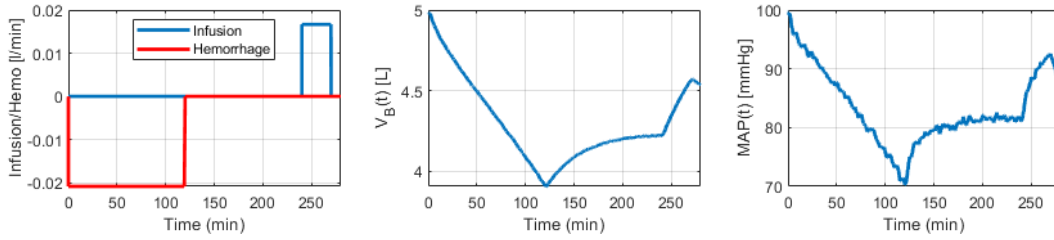
Figure 19:In-silico simulation scenario of a nominal subject

We can see from figure (19) that BV and MAP of the patient dropped to ~4.25L and ~82mmHg after hemorrhage (T=240 min). The goal of the control algorithm is to raise the blood pressure of the patient by 30mmHg. During step (1) of the control architecture which starts at time (T=240 min), a bolus infusion is administered to the patient. This raises the blood volume and MAP to ~4.5L and ~88mmHg respectively. The data collected between T=240 and T=280 min is used to individualize the hemodynamic model using equations (21) or (22) depending on measurement availability. Then, MRAC control is initiated and the blood pressure is raised by 30mmHg (82 to 112 mmHg) following a first order model trajectory with time constant of 15 min. Figures (20,21 and 22) show the infusion profile, MAP tracking performance and K_{map} online estimation results for the three versions of the control algorithm (equations 37,39 and 40) respectively.
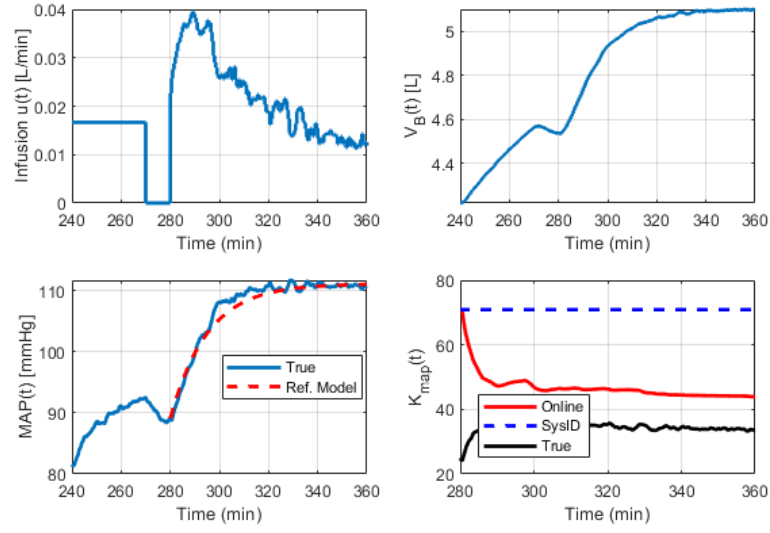
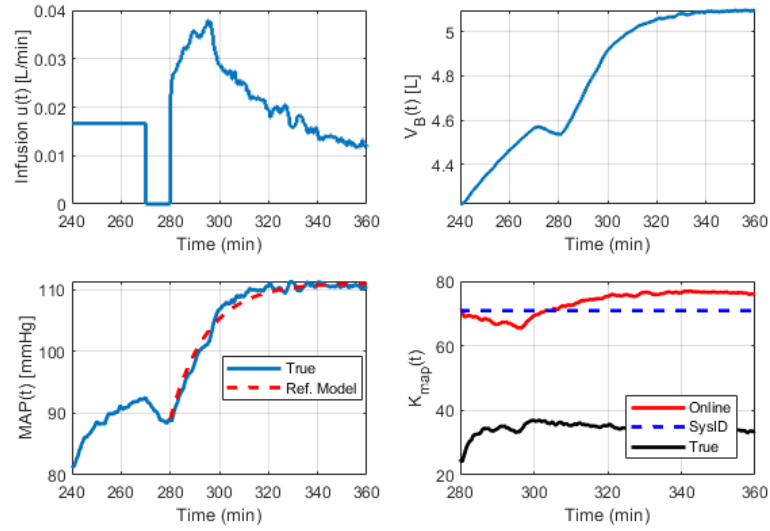*Figure 20: Tracking performance, infusion profile, and online estimation of K_{map} – plain MRAC scheme*

Figure 21: Tracking performance, infusion profile, and online estimation of K_{map} – single measurement CAC
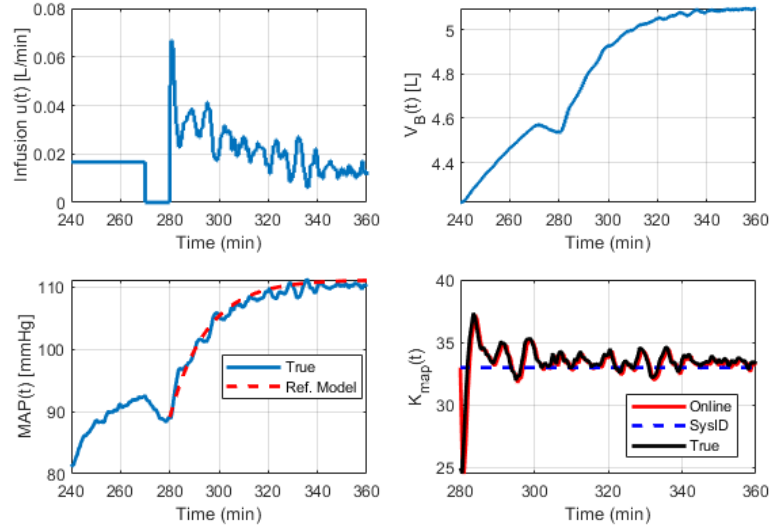
43

Figure 22: Tracking performance, infusion profile and online estimation of K_{map} – two measurement CAC

We can see from the figures above that tracking performance was achieved for all three versions of the control algorithm, while online estimation of K_{map} was only possible when both measurements (Hct and MAP) were available (figure 22). However, it performed slightly worse in terms of tracking as evident of the more oscillatory behavior of the response. This is due to the tracking-estimation tradeoff in adaptive control. When more noisy measurements are being fed to the adaptation law to get better estimates, worse tracking performance is observed [54].

From figures (20-21), contrary to what is expected by theory, plain MRAC scheme provided better online estimation performance than single-measurement composite adaptation scheme. This is due to the inaccurate estimates of α and K in the batch system identification step, which are used in the input prediction error composite term in equation (43). Further investigation supports this hypothesis. First, we realize that Guyton's model does not have K, α parameters explicitly so we try to find the "true" K

44

values by exciting the model using a rich signal (white noise) and performing system identification. "True" α is found by its definition $\alpha = \frac{\Delta V_{ISF}}{\Delta V_B}$. Table (3) shows a sample result for "true" vs estimated α, K. Second, we check our hypothesis by plugging in the "true" values in the input prediction error term in equation (43).

Table 3: True vs estimated K, α values for one virtual patient

	"True" values	**Batch SYSID results (eqn. 22)**
K	0.0380	0.15
α	3.1937	5.999
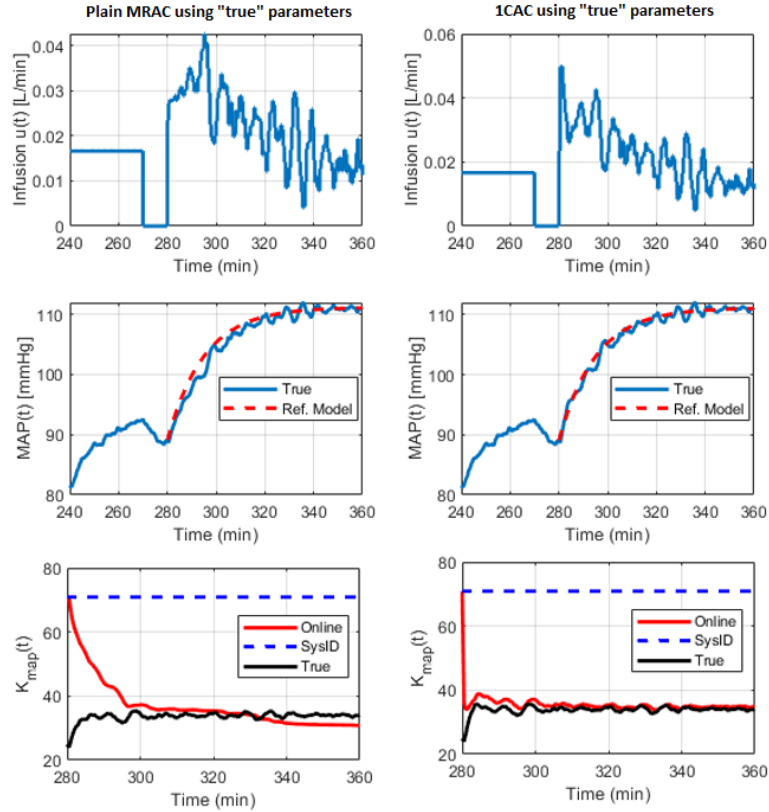
Figure 23: Comparison between the performance of single-measurement composite adaptation using "true" and estimated α and K

In figure (23), we can see that using "true" values we get better performance and online estimation than when using plain MRAC. This agrees with the discussion in 4.2.1.

In this chapter, we investigated the tracking and parameter estimation performance of a semi-adaptive controller under different measurement availability scenarios. Details of an in-silico test done on a highly nonlinear computer model of human cardiovascular system were shown. Results of the in-silico test on a nominal subject showed that our proposed control algorithm successfully tracked a first order reference model trajectory change in MAP. Moreover, depending on the quality and availability of measurements, we were able to estimate the time-varying parameter describing the relationship between BV and MAP. In the next chapter, we will provide a more detailed analysis of the results obtained from the in-silico testing over a cohort of 100 virtual patients and compare them from a statistical point of view.

Chapter 5: Results, Discussion and Conclusions

In chapter 4, we presented the in-silico testing scenario and provided the results on a nominal patient for the control architecture under different measurement availability scenarios. Here, we will discuss a more rigorous test of the controller by running similar simulations on a cohort of a 100 virtually generated patients as discussed in section (4.3). Obviously, it is not feasible to show the results for all 100 subjects, therefore, in this chapter we wish to quantify the tracking and estimation performance of the different versions of the adaptive controller. To do so, we analyze the results by conducting a statistical t-test and discuss the key features of the proposed controllers.

5.1 Performance Error Metrics

To quantify both tracking and estimation performance, we ought to use a common metric to evaluate the performance of computer-controlled infusion pumps, better known as Performance Error (PE) metrics [55]. In quantifying tracking performance of a controller, performance error is defined as the ratio of the discrepancy between reference model and actual MAP values, to the actual MAP values.

$$PE = \frac{y_m - y}{y} \cdot 100\% \tag{44}$$

For quantifying online $K_{map}(t)$ estimation, performance error metric is defined as the ratio of the discrepancy between "true" $K_{map}(t)$ value and estimated $1/\theta(t)$ to the estimated $1/\theta(t)$.

$$PE = \frac{K_{map}(t) - 1/\theta(t)}{1/\theta(t)} \cdot 100\% \tag{45}$$

Equations (44, 45) are used to define the following four measures, for the case of tracking and estimation independently: (i) Median Absolute Performance Error (MDAPE) which is a measure of inaccuracy.

$$MDAPE = \text{median}\,\{|PE|\} \tag{46}$$

(ii) Median Performance Error (MDPE): a measure of "bias". This a signed value and represents how much the output (or parameter) overshot or undershot its true values.

$$MDPE = \text{median}\,\{PE\} \tag{47}$$

(iii) Divergence: the slope obtained from linear regression of the absolute PE against time. This measure describes the time-related trend of the actual versus estimated values.

$$\text{Divergence} = \frac{(\sum_{i=1}^{N}|PE_i| \cdot t_i) - (\sum_{i=1}^{N}|PE_i|)(\sum_{i=1}^{N} t_i)/N}{\sum_{i=1}^{N} t_i^2 - (\sum_{i=1}^{N} t_i)^2/N} \tag{48}$$

(iv) Wobble: a measure of inter-subject variability as well as an indicator of time-related changes in tracking or estimation performance.

$$\text{Wobble} = \text{median}\,\{|PE - MDPE|\} \tag{49}$$

5.2 Tracking Performance Results

In this section, we will compare the tracking performance of all three versions of the proposed controller. We begin by using equation (44) to calculate the PE, then evaluate the four metrics explained in section 5.1. In particular, for every patient of the 100 virtual patients, we run the in-silico simulation and collect the output data (y_2) as well as (y_m) then calculate MDAPE, MDPE, Divergence and Wobble for each patient.

48

Finally, the results of each controller for all subjects are reported in Table (5) which shows the mean and standard deviation of all the results.

Table 4: Summary of performance error metrics for tracking performance

Metric (mean +/- SD)	2-measurement adaptation scheme	Single-measurement adaptation scheme	Plain MRAC
MDAPE [%]	2.886 +/- (1.007)	2.546 +/- (0.72)	2.507 +/- (0.829)
MDPE [%]	1.741+/- (1.399)	-0.698 +/- (1.695)	-1.474 +/- (1.201)
Divergence [%/min]	-0.082+/- (0.042)	-0.096 +/- (0.063)	-0.096 +/- (0.066)
Wobble [%]	2.043+/- (0.368)	2.498 +/- (0.829)	2.417 +/- (0.836)

The results suggest that the tracking accuracy (MDAPE) of the three controllers, although comparable, was significantly different depending on measurement availability. Generally, the controller was able to track a first order model change to a desired set point successfully. However, when more information is fed to the controller, tracking performance slightly deteriorates in exchange of enhanced estimation. MDPE results suggest that 2-measurement adaptation scheme overshot (on average) the predetermined set point, while single-measurement schemes undershot it. Divergence was not significantly different between the three controllers, indicating that there were no abnormal time trends and that all controllers successfully tracked the first order model trajectory. Finally, results also show how 2-measurement adaptation scheme was significantly better in adapting to inter-subject variability as measured by the Wobble metric. To make such a conclusion, the following t-test provide a better insight. Using MATLAB's (Mathworks, Natick, MA) one-way analysis of variance tools "`ANOVA1`" and "`multicompare`", we got the results of pairwise comparison results for the four

metrics (MDAPE, MDPE, Divergence and Wobble). Figures (24-27) show the results
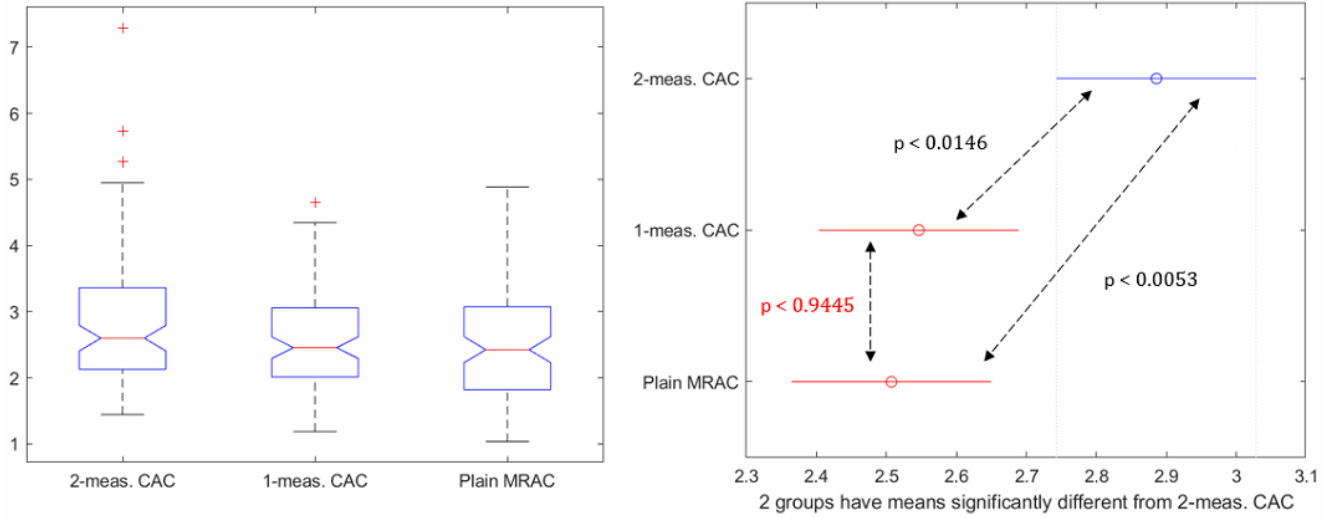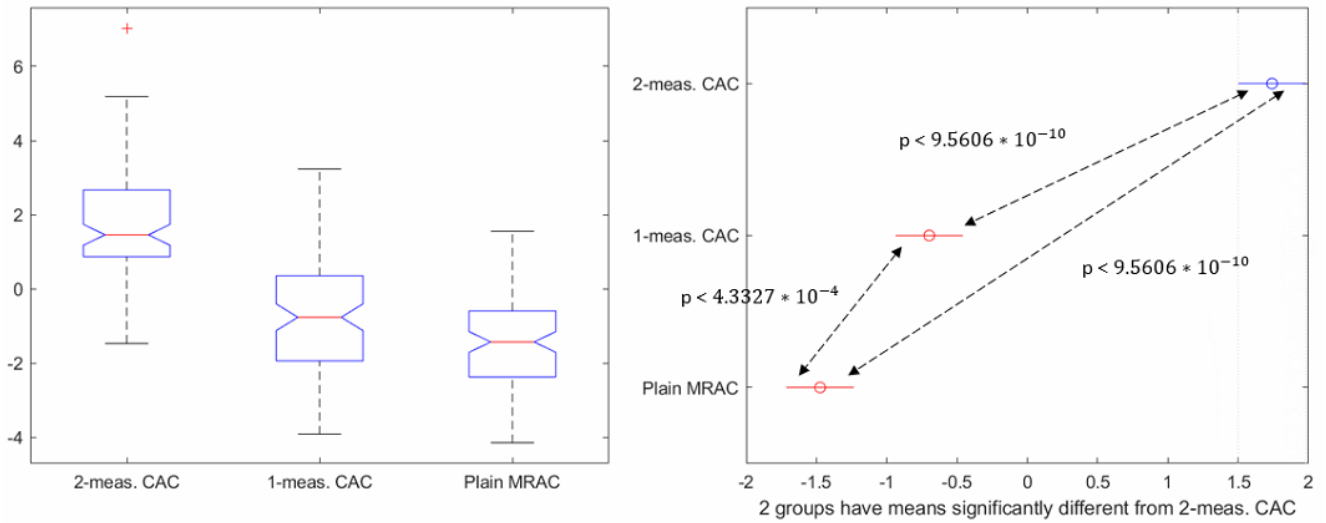
of this analysis.

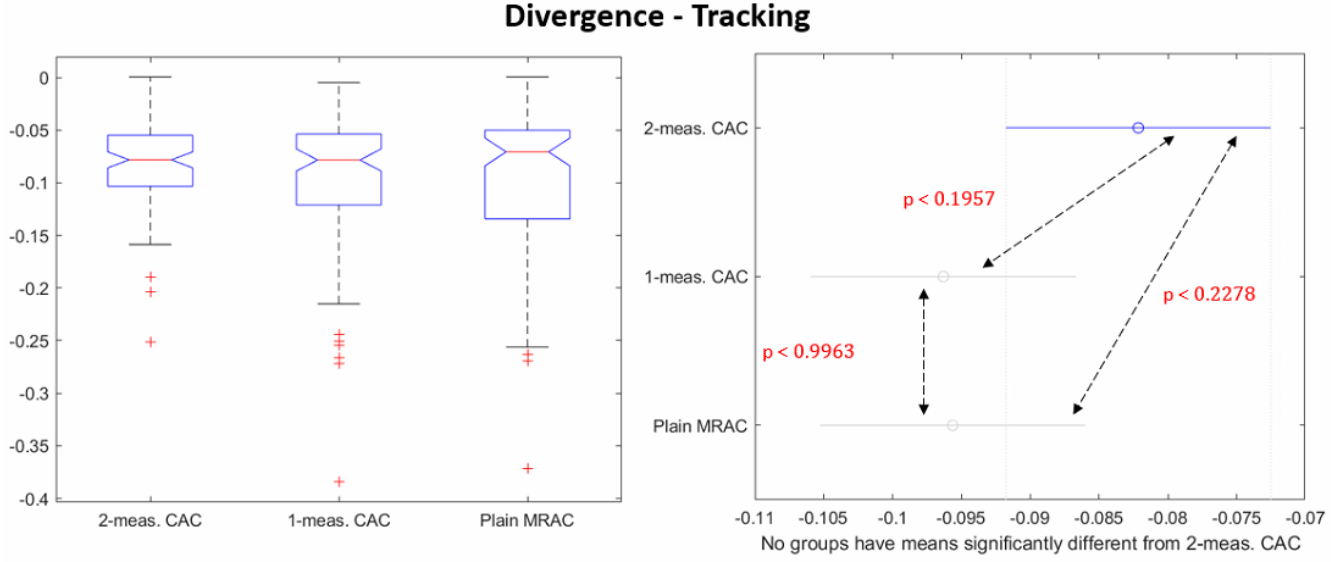*Figure 24: Statistical t-test results for tracking performance MDAPE metric*

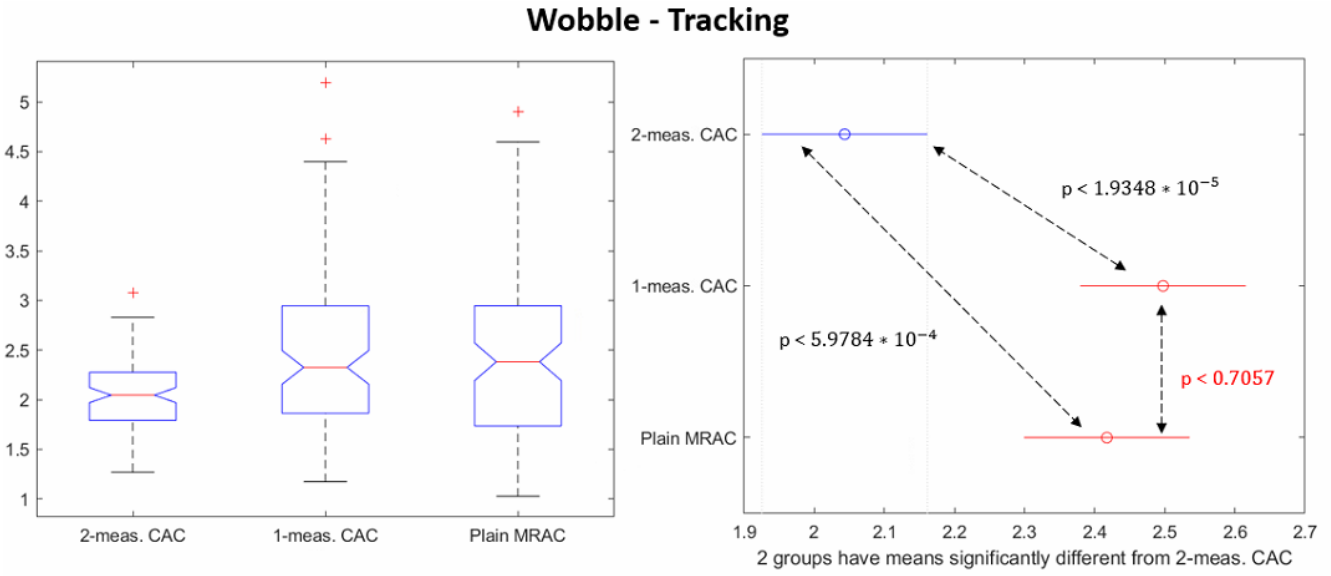*Figure 25: Statistical t-test results for tracking performance MDPE metric*

Divergence - Tracking

Figure 26: Statistical t-test results for tracking performance Divergence metric

Wobble - Tracking

Figure 27: Statistical t-test results for tracking performance Wobble metric

5.3 Estimation Performance Results

In this section, we quantify the online estimation performance of the three adaptation schemes. The same performance error metrics are followed, that is: we use equation (45) to calculate PE, then evaluate MDAPE, MDPE, Divergence and Wobble

51

for each patient. Following the same procedure in 5.2, the table below lists the mean and standard deviation of the PE metrics for all three adaptation schemes.

Table 5: Summary of performance error metrics for estimation performance

Metric (mean +/- SD)	2-measurement adaptation scheme	Single-measurement adaptation scheme	Plain MRAC
MDAPE [%]	0.051 +/- (0.032)	0.517 +/- (0.052)	0.331 +/- (0.119)
MDPE [%]	0.031 +/- (0.051)	-0.517 +/- (0.052)	-0.326 +/- (0.132)
Divergence [%/min]	0.000 +/- (0.000)	0.001 +/- (0.001)	-0.001 +/- (0.001)
Wobble [%]	0.009 +/- (0.001)	0.021 +/- (0.007)	0.015 +/- (0.006)

The results suggest that availability of two measurements is best for online estimation, which is expected because we have more information about the system. However, as opposed to what is expected by the theory presented in chapter 3, the plain MRAC provides better estimates for online estimation of $K_{map}(t)$ rather than the single-measurement composite adaptation scheme. This is due to the presence of inaccurate α, K in the input prediction error composite term that caused deteriorated estimate of $\theta(t)$ and hence $K_{map}(t)$ (see discussion in section 4.4). Also, we can see from table (5) that divergence metric for 2-measurement composite adaptation scheme was 0, which indicates that we managed to maintain perfect online parameter estimation for all subjects as indicated by the wobble metric as well (the estimation algorithm also adapted to inter0subject variability). To further analysis this hypothesis, we conducted a one-way analysis of variance test, the results of which are presented in the figures below.
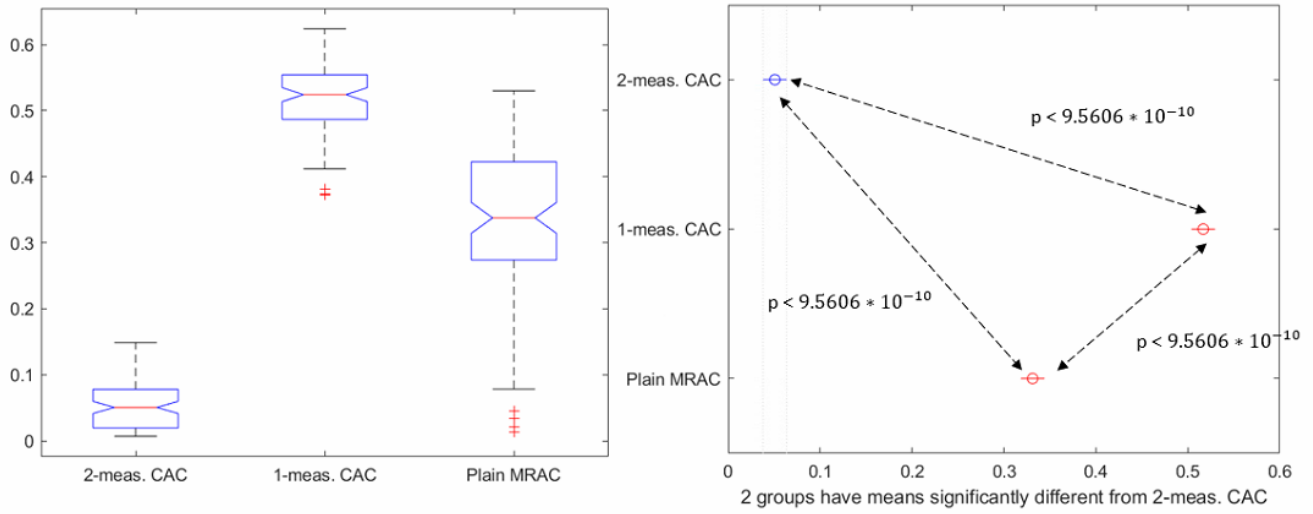
Figure 28: Statistical t-test results for estimation performance MDAPE metric
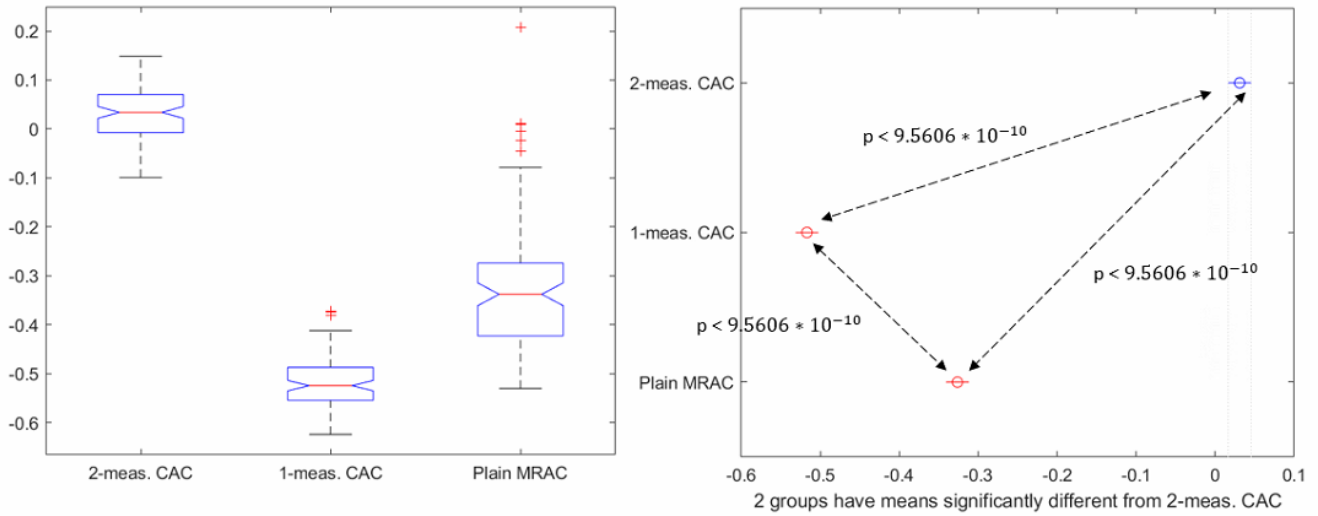

Figure 29: Statistical t-test results for estimation performance MDPE metric
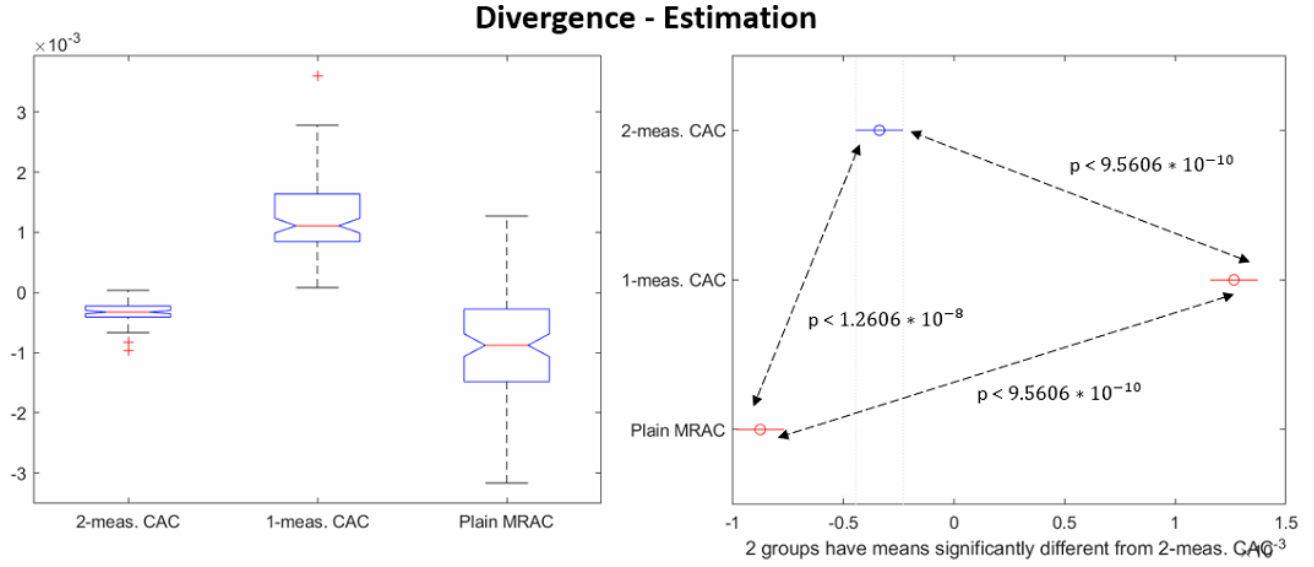
53

Figure 30: Statistical t-test results for estimation performance Divergence metric
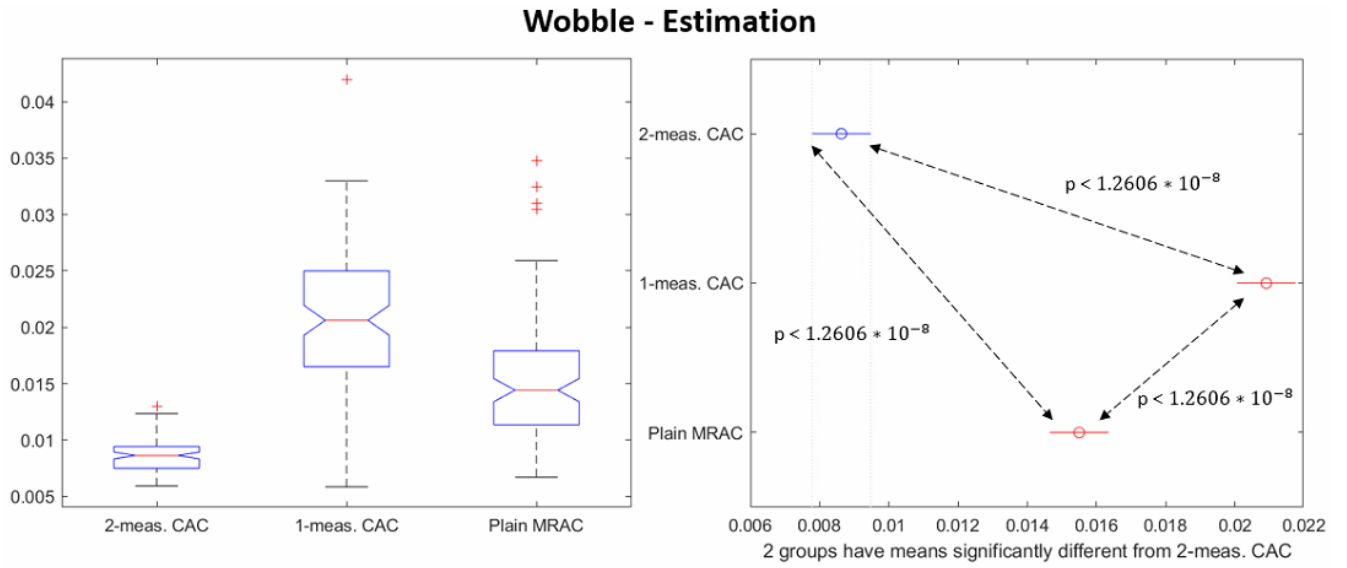

Figure 31: Statistical t-test results for estimation performance Wobble metric

5.4 Conclusions and Discussion

In this work, we proposed an extension to an existing hemodynamic model of blood volume response to fluid infusion to include mean arterial pressure response to blood volume perturbation. We used this 5-parameter linear model to develop three

versions of a two-step semi-adaptive closed loop control algorithm for the development of an autonomous fluid resuscitation system and investigated them under different measurement availability scenarios. To evaluate the performance of the control algorithms, we conducted an in-silico test on a highly non-linear, well-established computer model of cardiovascular system (Guyton's model) on a cohort of 100 virtually generated patients. The virtual patients were generated by randomly perturbing eight key parameters of the model within a physiological range. The results were presented in chapter 4, and the following two points were observed:

1) The use of two-measurements adaptation scheme provides slightly worse (more oscillatory) tracking performance to reference model trajectories, than when using single-measurement adaptation schemes.

2) The use of two-measurements adaptation scheme provides better (perfect) online estimation of model parameter $K_{map}(t)$, than when using single-measurement adaptation schemes.

These two points indicate that a trade-off between tracking and estimation performance exists in adaptive control algorithms. This is due to the adaptation-noise rejection tradeoff in the adaptation algorithm and the fact that the two-measurement adaptation scheme is exposed to more error sources than its counterparts.

Statistical test done on results of an in-silico test of the control algorithm for 100 virtual patients, supports the existence of such trade-off between tracking and estimation performance. The deterioration in tracking performance, although small in terms of performance error (average increase of ~0.3%), was significant when compared to the tracking performance of single-measurement schemes (p<0.015).

5.5 Future Work

The extension of the hemodynamic model to include mean arterial pressure response to blood volume perturbations was described using a time-varying parameter $K_{map}(t)$, which is intended to capture the sensitivity of SV and E_a changes to BV changes. One important assumption in the development of this control algorithm was the assumption that $K_{map}(t)$ is generally positive during fluid resuscitation. However, this assumption is not true for subjects that are not responsive to fluid resuscitation. This is one limitation of the case of single-measurement adaptation scheme, which will be addressed in future work. Second, physiological interpretability was not strictly made since $K_{map}(t)$ describes the responsiveness of the patient to fluid infusion and it does not have an exact counterpart in physiology literature. However, it is physiologically plausible: for example, high $K_{map}(t)$ values indicate high responsiveness of MAP during fluid infusion.

Online estimation of $K_{map}(t)$ is useful for learning more about the responsiveness of the patient to fluid infusion. This can be incorporated in the design of an autonomous set point selection controller where the need for the clinician to enter a specified set point is not required, but rather a set of upper and lower bounds that should not be exceeded. To get almost perfect estimates of $K_{map}(t)$, we require the availability of both MAP measurements and Hct measurement, which highly affects the estimates of V_{B0}^* in equation (39). Hct measurements are hard to obtain in clinical scenarios but would be achievable with the advancement of blood volume monitoring and measuring devices.

Finally, this controller can potentially be used in a Hardware-in-the-Loop (HIL) test to evaluate the robustness and accuracy of such controllers under more practical scenarios.
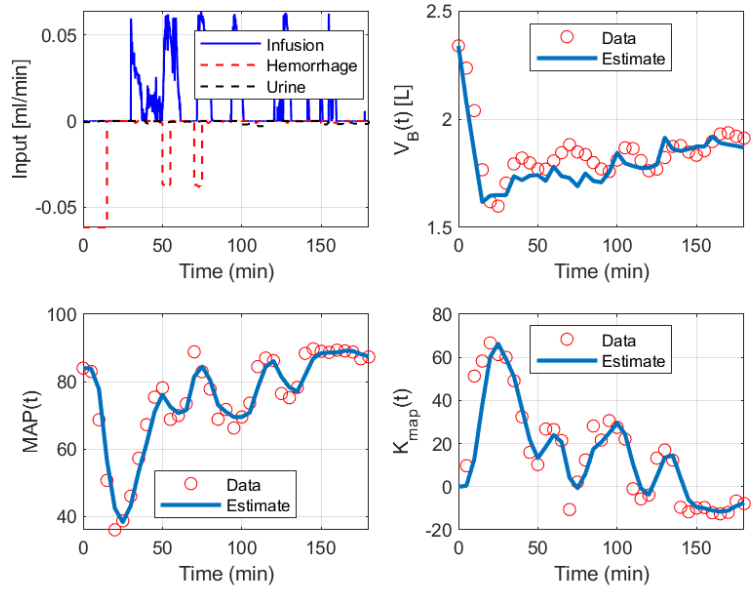
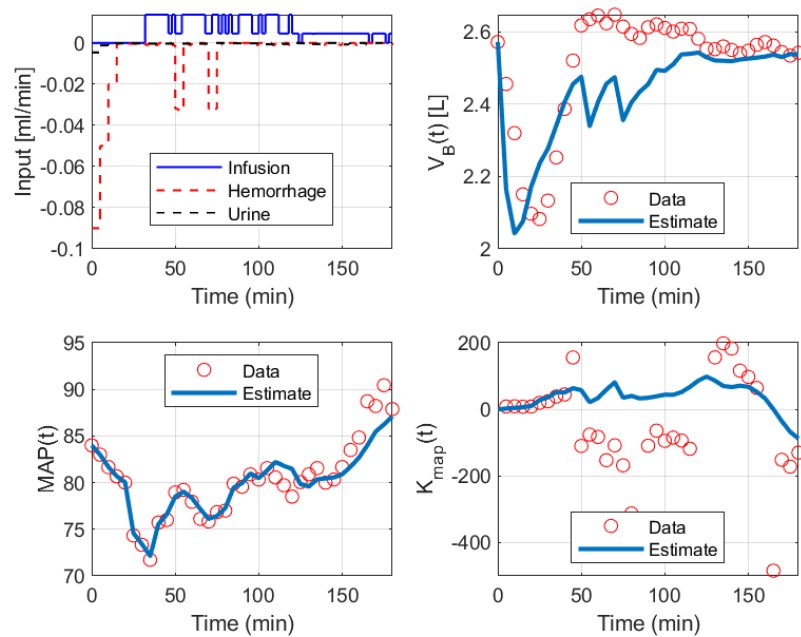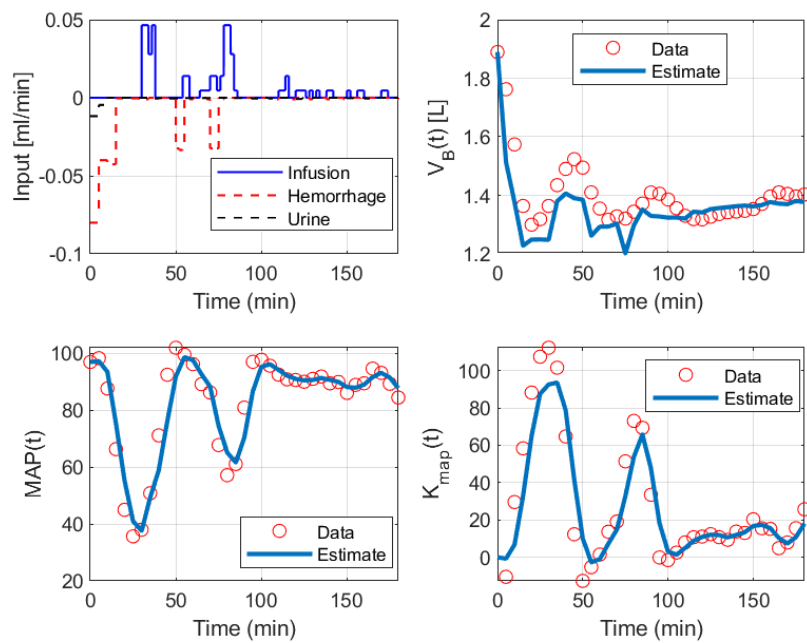# Appendices

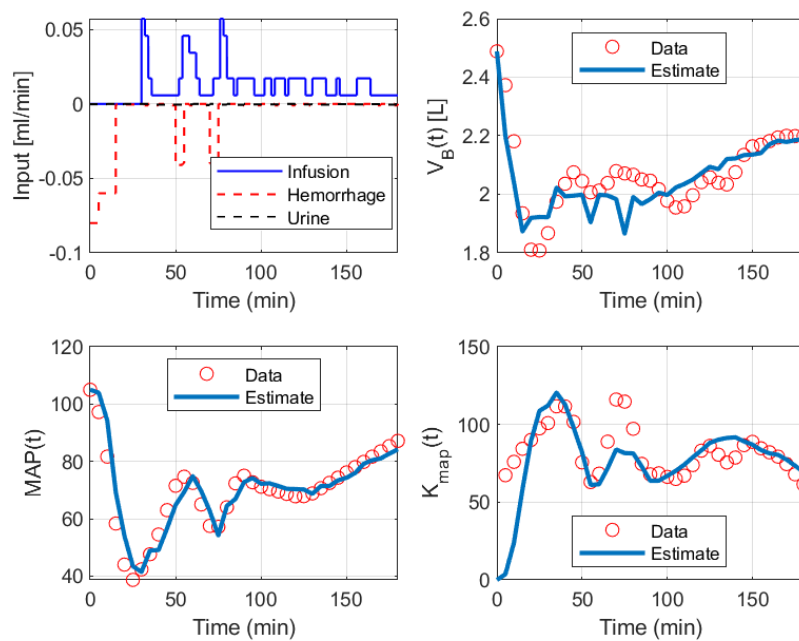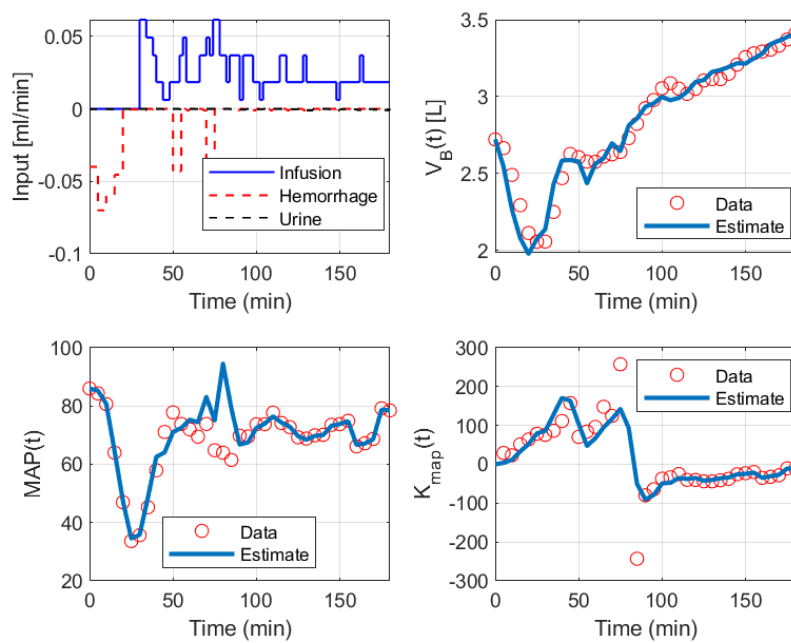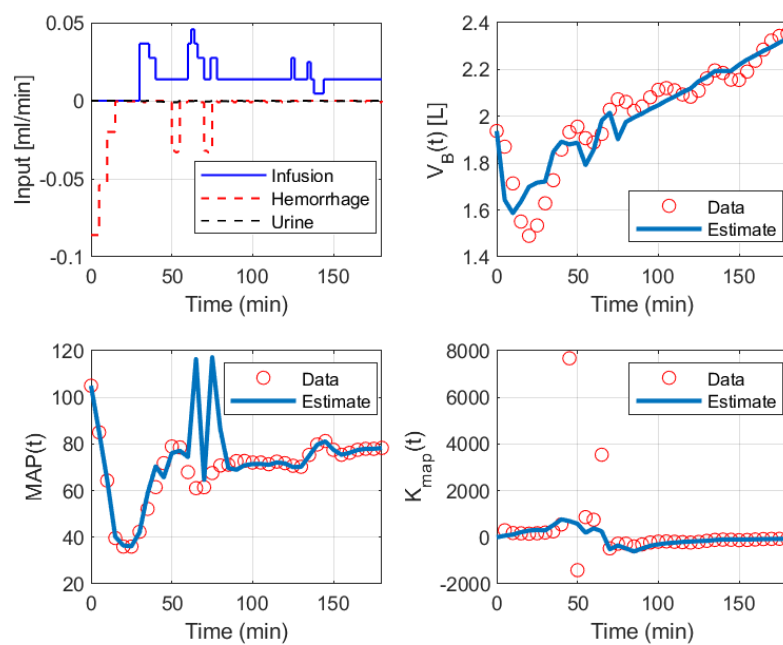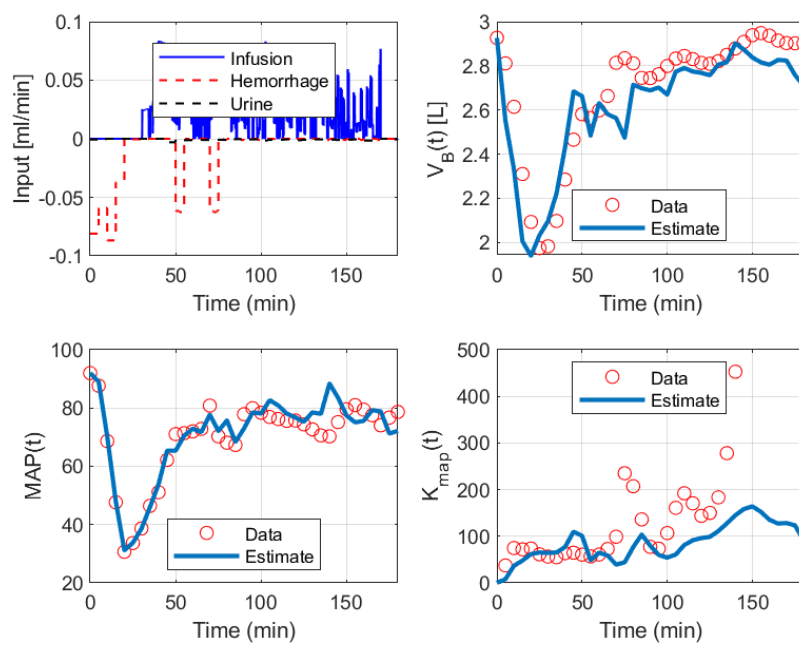## Appendix (A): Model Fitting Results to Experimental Data

Sheep 1
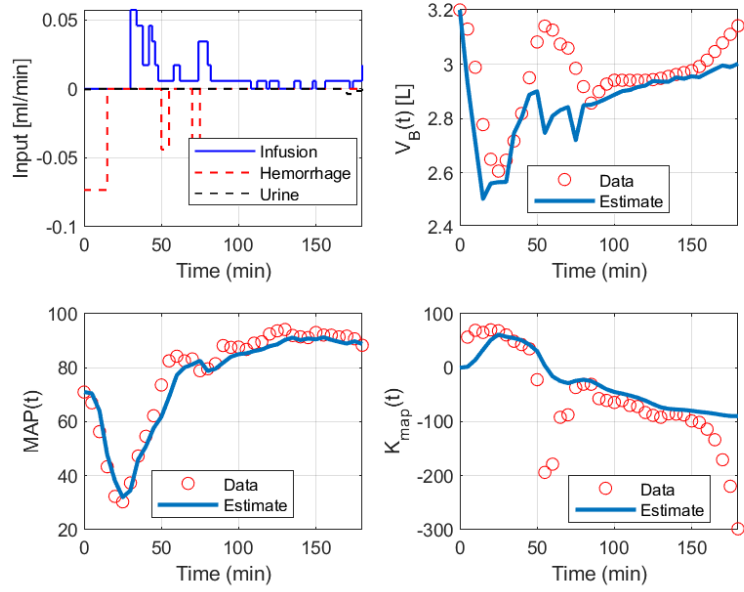
Sheep 2

Sheep 3

Sheep 4

Sheep 5

Sheep 6

Sheep 7

Sheep 8

Sheep 9
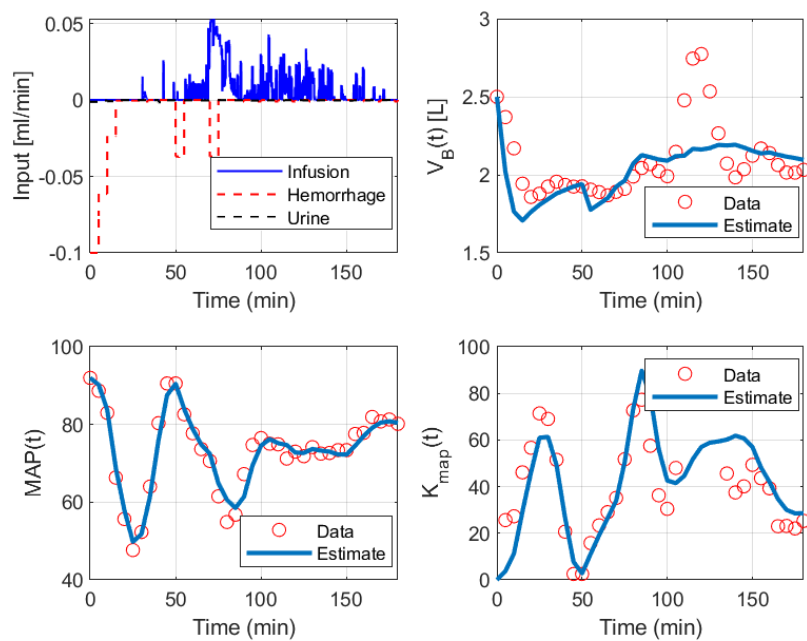
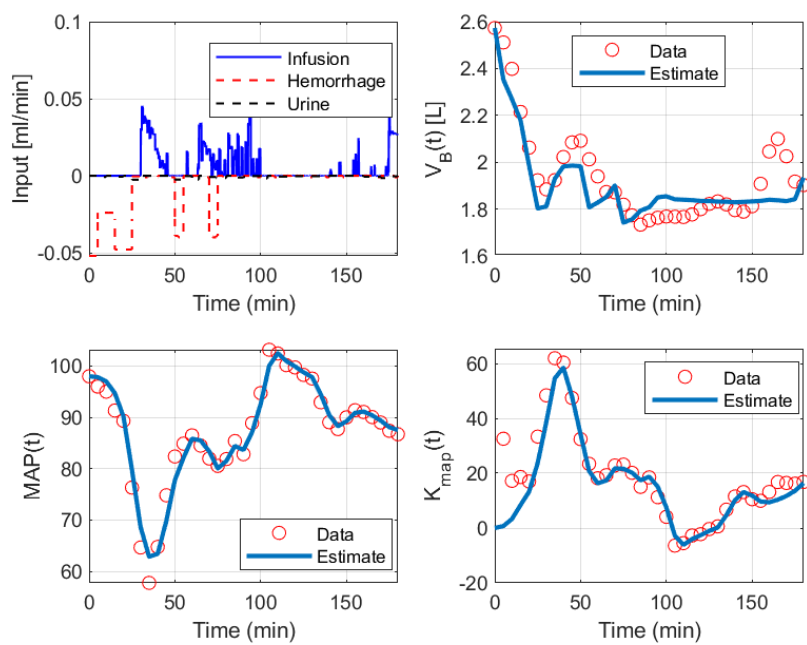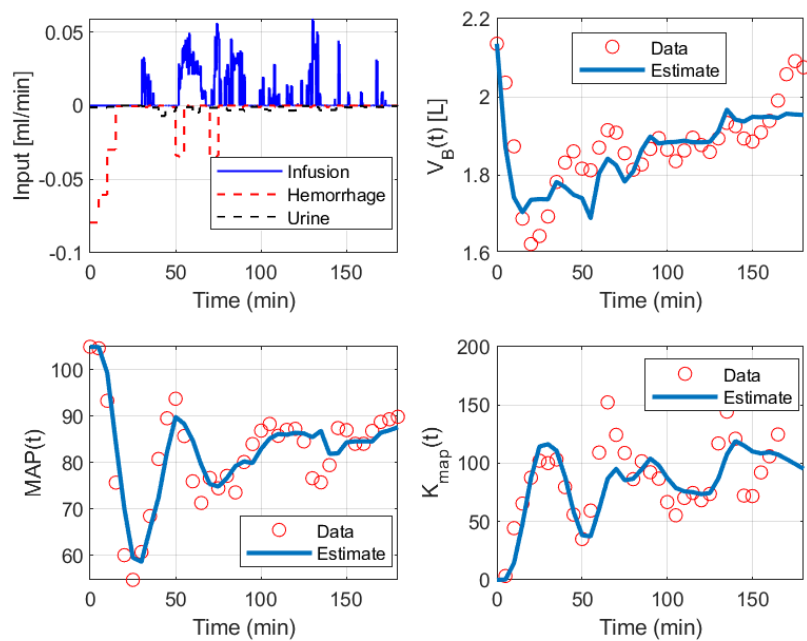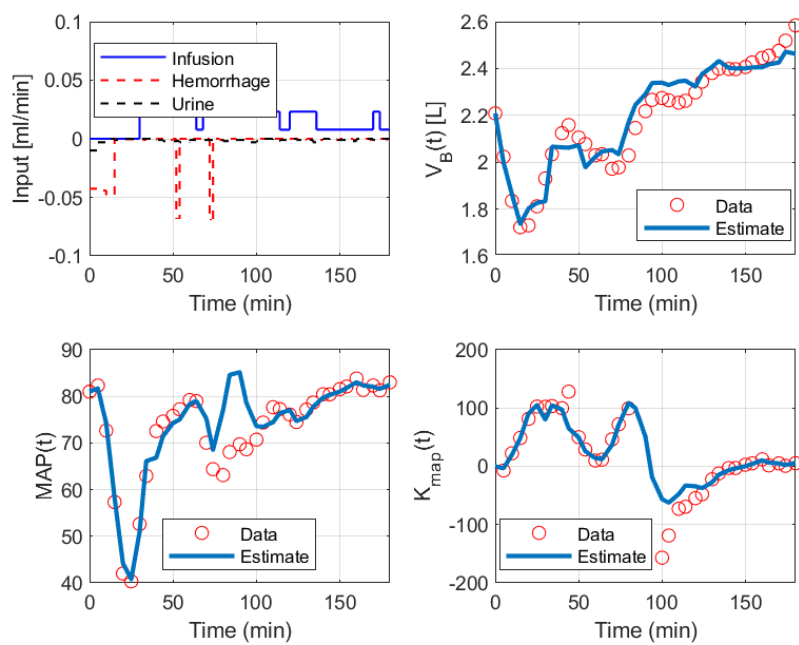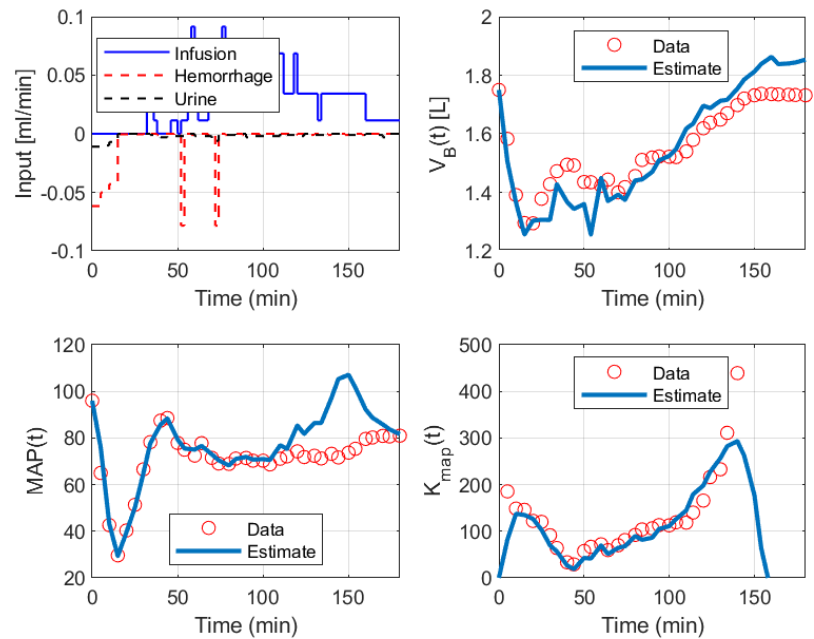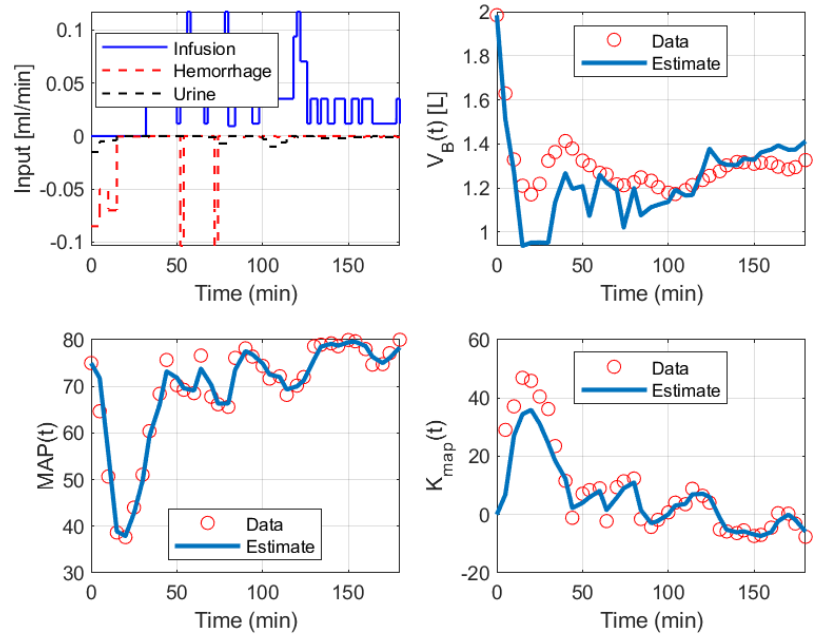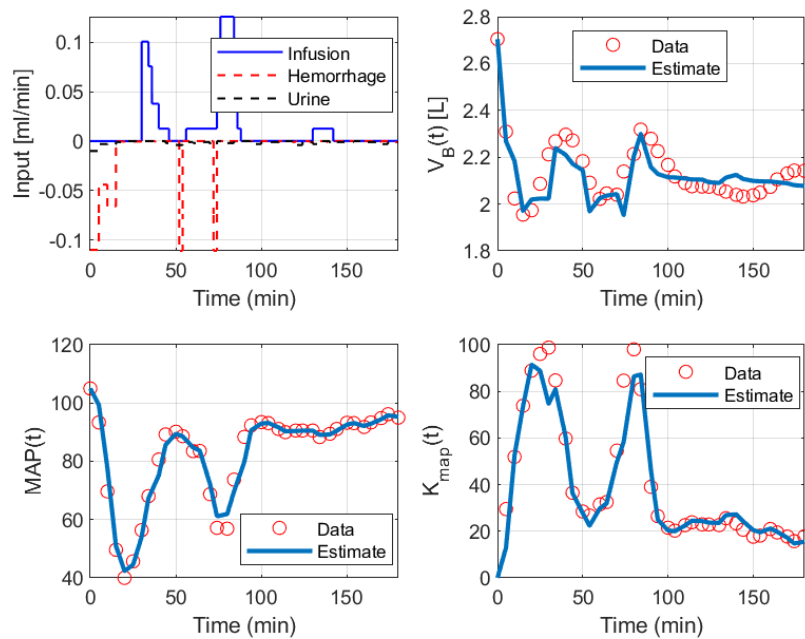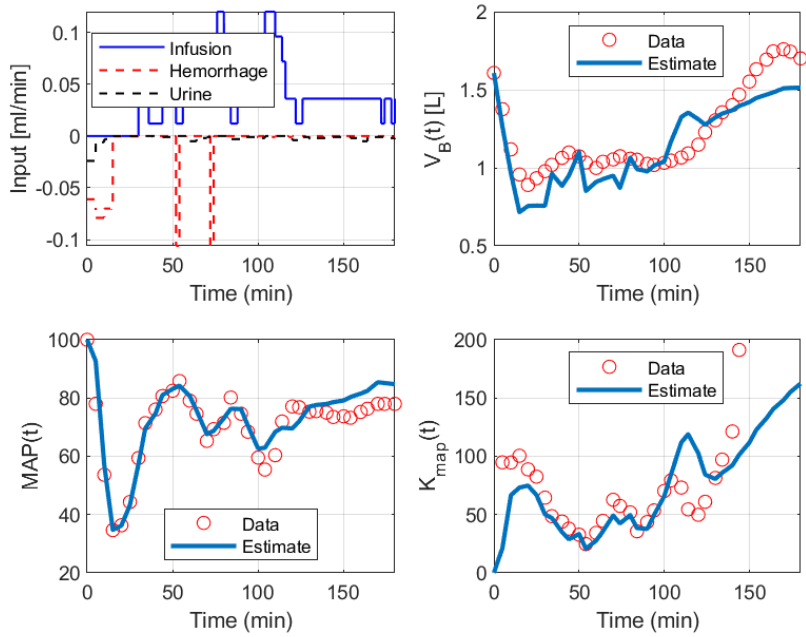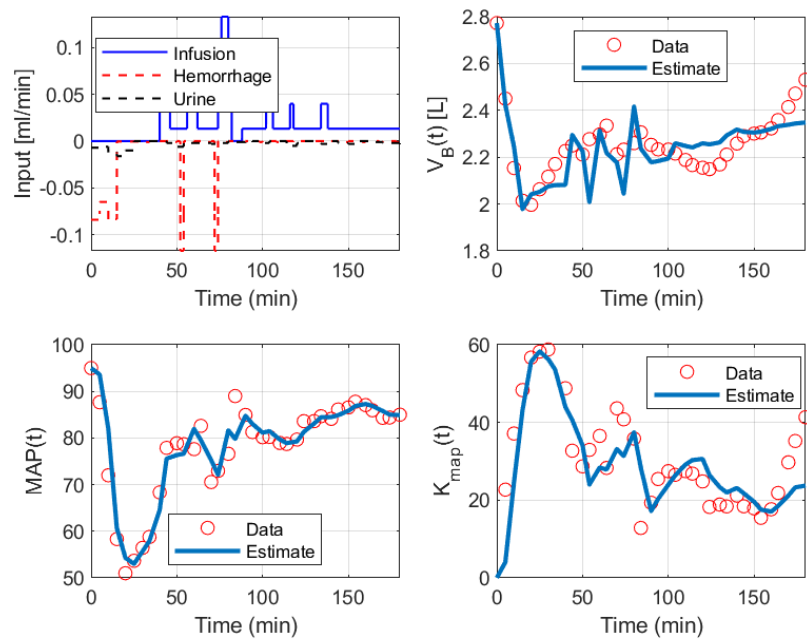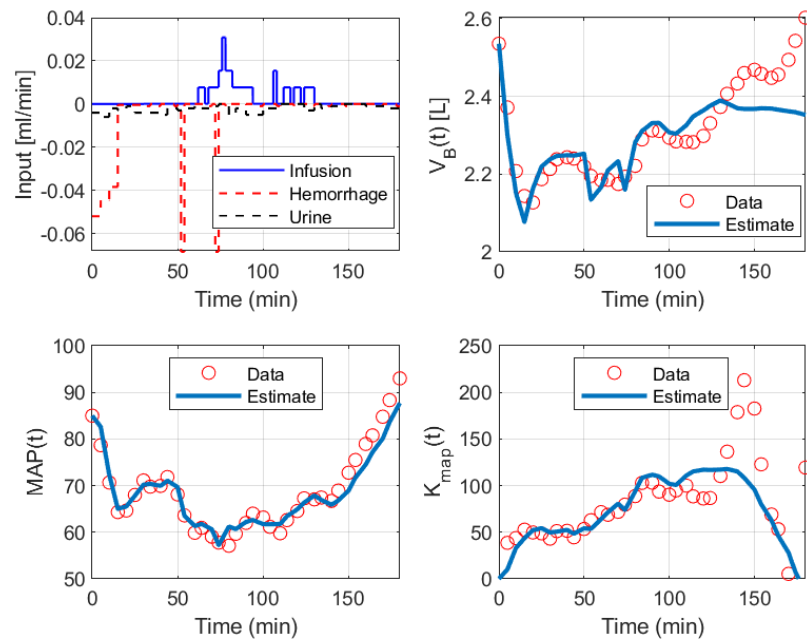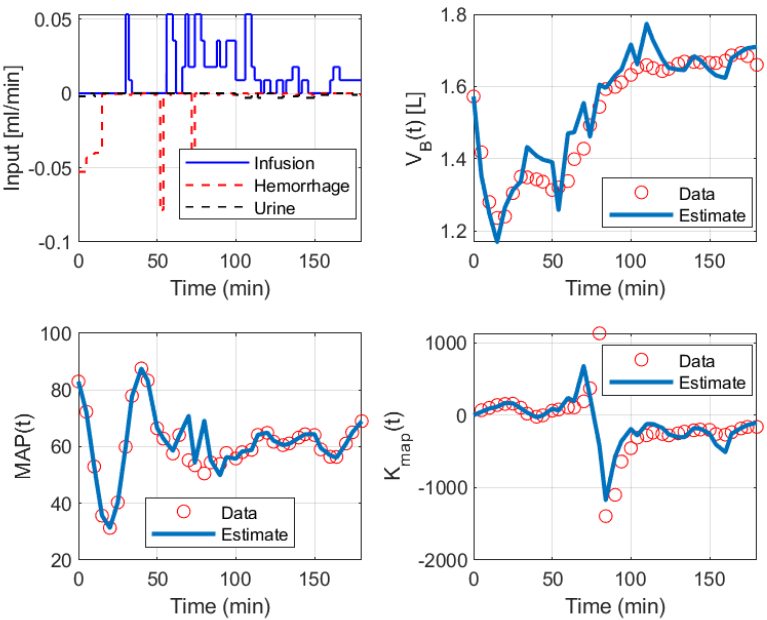Sheep 10

Sheep 11

Sheep 12

Sheep 13

Sheep 14
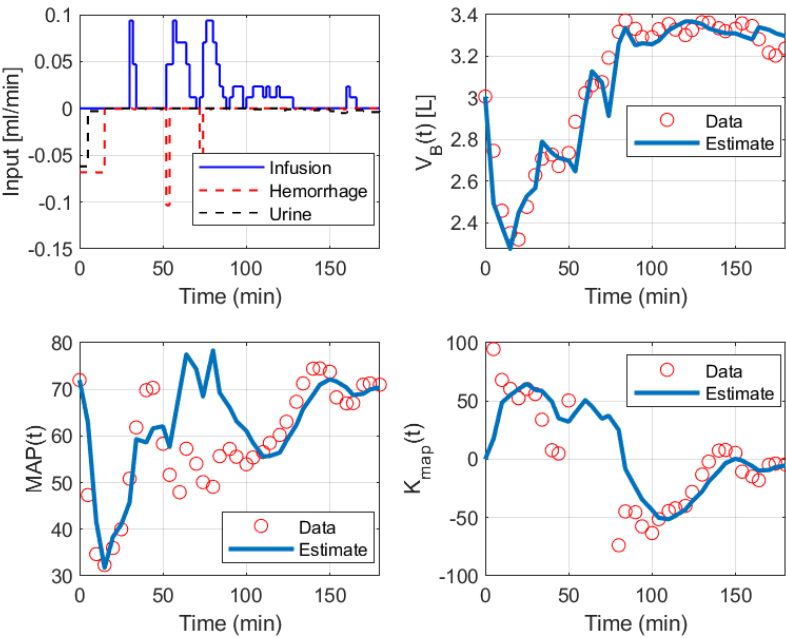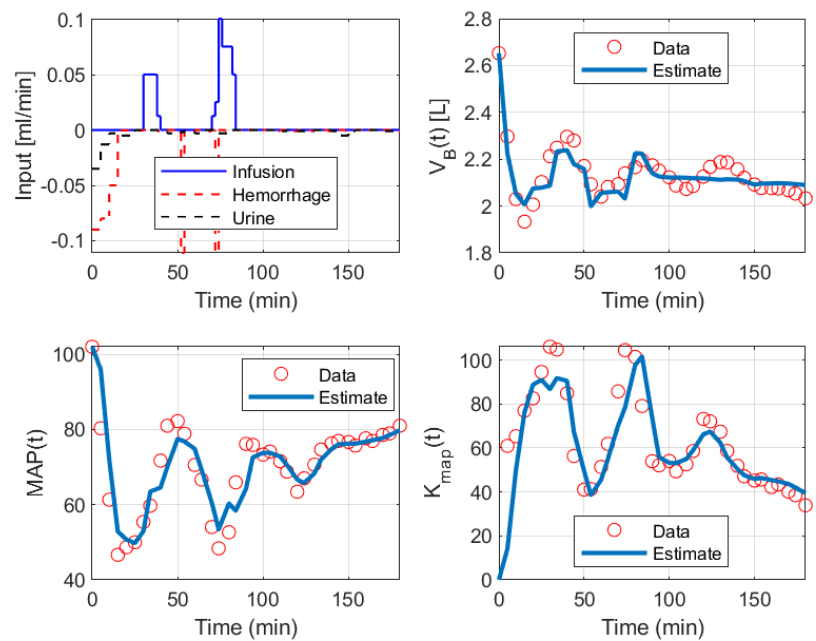
Sheep 15

Sheep 16

Sheep 17
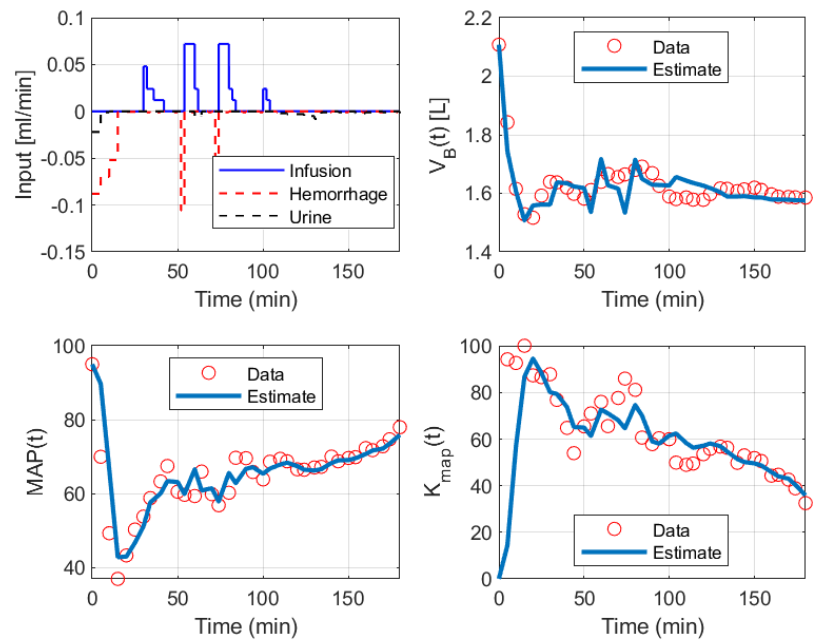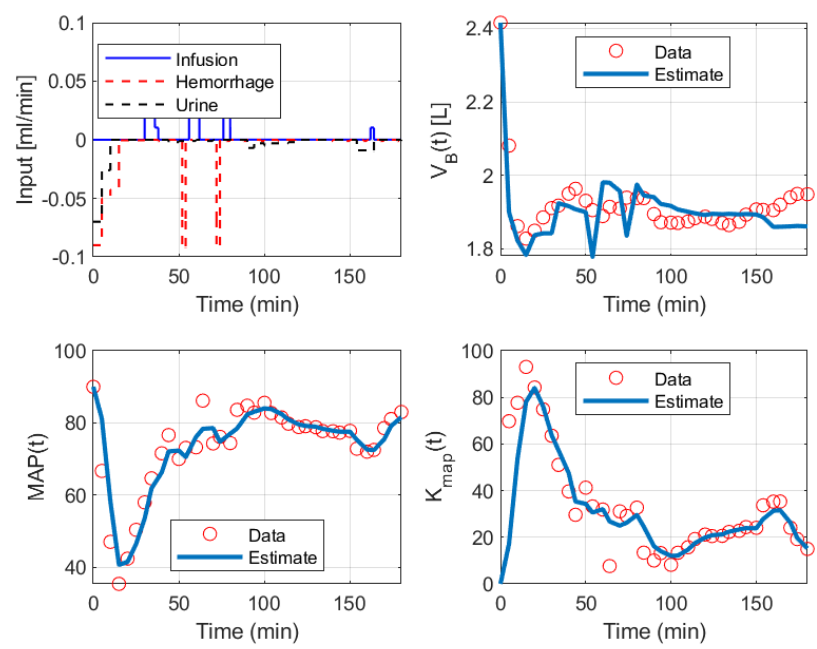
Sheep 18

Sheep 19

Sheep 20

Sheep 21

Sheep 22

68

Sheep 23

Bibliography

[1] V. Chatrath, R. Khetarpal, and J. Ahuja, "Fluid management in patients with trauma: Restrictive versus liberal approach," *J. Anaesthesiol. Clin. Pharmacol.*, vol. 31, no. 3, p. 308, 2015, doi: 10.4103/0970-9185.161664.

[2] B. Rochwerg *et al.*, "Fluid Resuscitation in Sepsis: A Systematic Review and Network Meta-analysis," *Ann. Intern. Med.*, vol. 161, no. 5, p. 347, Sep. 2014, doi: 10.7326/M14-0178.

[3] A. Bouglé, A. Harrois, and J. Duranteau, "Resuscitative strategies in traumatic hemorrhagic shock," *Ann. Intensive Care*, vol. 3, no. 1, p. 1, Jan. 2013, doi: 10.1186/2110-5820-3-1.

[4] M. Haberal, A. E. Abali, and H. Karakayali, "Fluid management in major burn injuries," *Indian J. Plast. Surg.*, vol. 43, no. 3, p. 29, 2010, doi: 10.4103/0970-0358.70715.

[5] I. of Medicine and C. on F. R. for C. Casualties, *Fluid Resuscitation: State of the Science for Treating Combat Casualties and Civilian Injuries*. National Academies Press, 1999.

[6] S. A. Tisherman *et al.*, "Clinical Practice Guideline: Endpoints of Resuscitation," *J. Trauma Acute Care Surg.*, vol. 57, no. 4, pp. 898–912, Oct. 2004, doi: 10.1097/01.TA.0000133577.25793.E5.

[7] K. K. Varadhan and D. N. Lobo, "A meta-analysis of randomised controlled trials of intravenous fluid therapy in major elective open abdominal surgery: getting the balance right," *Proc. Nutr. Soc.*, vol. 69, no. 4, pp. 488–498, Nov. 2010, doi: 10.1017/S0029665110001734.

[8] A. C. de Oliveira, P. C. Garcia, L. de S. Nogueira, A. C. de Oliveira, P. C. Garcia, and L. de S. Nogueira, "Nursing workload and occurrence of adverse events in intensive care: a systematic review," *Rev. Esc. Enferm. USP*, vol. 50, no. 4, pp. 683–694, Aug. 2016, doi: 10.1590/S0080-623420160000500020.

[9] Y. Peeters, S. Vandervelden, R. Wise, and M. L. N. G. Malbrain, "An overview on fluid resuscitation and resuscitation endpoints in burns: Past, present and future. Part 1 - historical background, resuscitation fluid and adjunctive treatment," *Anaesthesiol. Intensive Ther.*, vol. 47 Spec No, pp. s6-14, 2015, doi: 10.5603/AIT.a2015.0063.

[10] J. Rinehart, C. Lee, M. Cannesson, and G. Dumont, "Closed-Loop Fluid Resuscitation: Robustness Against Weight and Cardiac Contractility Variations," *Anesth. Analg.*, vol. 117, no. 5, pp. 1110–1118, Nov. 2013, doi: 10.1213/ANE.0b013e3182930050.

[11] J. Salinas *et al.*, "Closed-Loop and Decision-Assist Resuscitation of Burn Patients:," *J. Trauma Inj. Infect. Crit. Care*, vol. 64, no. Supplement, pp. S321–S332, Apr. 2008, doi: 10.1097/TA.0b013e31816bf4f7.

[12] S. L. Hoskins *et al.*, "Closed-Loop Resuscitation of Burn Shock," *J. Burn Care Res.*, vol. 27, no. 3, pp. 377–385, May 2006, doi: 10.1097/01.BCR.0000216512.30415.78.

[13]   H. Ying and L. C. Sheppard, "Real-time expert-system-based fuzzy control of mean arterial pressure in pigs with sodium nitroprusside infusion," *Med. Prog. Technol.*, vol. 16, no. 1–2, pp. 69–76, May 1990.

[14]   S. R. Abram, B. L. Hodnett, R. L. Summers, T. G. Coleman, and R. L. Hester, "Quantitative Circulatory Physiology: an integrative mathematical model of human physiology for medical education," *Adv. Physiol. Educ.*, vol. 31, no. 2, pp. 202–210, Jun. 2007, doi: 10.1152/advan.00114.2006.

[15]   J. Kofránek and J. Rusz, "Restoration of Guyton´s diagram for regulation of the circulation as a basis for quantitative physiological model development," *Physiol. Res.*, vol. 59, no. 6, pp. 897–908, 2010.

[16]   T. A. Parlikar, T. Heldt, G. V. Ranade, and G. C. Verghese, "Model-based estimation of cardiac output and total peripheral resistance," in *2007 Computers in Cardiology*, Sep. 2007, pp. 379–382, doi: 10.1109/CIC.2007.4745501.

[17]   J. C. Pirkle and D. S. Gann, "Restitution of blood volume after hemorrhage: role of the adrenal cortex," *Am. J. Physiol.*, vol. 230, no. 6, pp. 1683–1687, Jun. 1976, doi: 10.1152/ajplegacy.1976.230.6.1683.

[18]   G. Arturson, T. Groth, A. Hedlund, and B. Zaar, "Computer simulation of fluid resuscitation in trauma. First pragmatic validation in thermal injury," *J. Burn Care Rehabil.*, vol. 10, no. 4, pp. 292–299, Aug. 1989, doi: 10.1097/00004630-198907000-00002.

[19]   A. Hedlund, B. Zaar, T. Groth, and G. Arturson, "Computer simulation of fluid resuscitation in trauma. I. Description of an extensive pathophysiological model and its first validation," *Comput. Methods Programs Biomed.*, vol. 27, no. 1, pp. 7–21, Aug. 1988, doi: 10.1016/0169-2607(88)90099-5.

[20]   F. Saito, T. Shimazu, J. Miyamoto, T. Maemura, and M. Satake, "Interstitial fluid shifts to plasma compartment during blood donation: Interstitial Fluid Shift during Donation," *Transfusion (Paris)*, vol. 53, no. 11, pp. 2744–2750, Nov. 2013, doi: 10.1111/trf.12120.

[21]   A. Hirshberg, D. B. Hoyt, and K. L. Mattox, "Timing of Fluid Resuscitation Shapes the Hemodynamic Response to Uncontrolled Hemorrhage: Analysis Using Dynamic Modeling:," *J. Trauma Inj. Infect. Crit. Care*, vol. 60, no. 6, pp. 1221–1227, Jun. 2006, doi: 10.1097/01.ta.0000220392.36865.fa.

[22]   S. H. Simpson, G. Menezes, S. N. Mardel, S. Kelly, R. White, and T. Beattie, "A computer model of major haemorrhage and resuscitation," *Med. Eng. Phys.*, vol. 18, no. 4, pp. 339–343, Jun. 1996, doi: 10.1016/1350-4533(95)00044-5.

[23]   S. N. Mardel, S. H. Simpson, S. Kelly, R. Wytch, T. F. Beattie, and G. Menezes, "Validation of a computer model of haemorrhage and transcapillary refill," *Med. Eng. Phys.*, vol. 17, no. 3, pp. 215–218, Apr. 1995, doi: 10.1016/1350-4533(95)95712-J.

[24]   R. L. Wears and C. N. Winton, "Load and go versus stay and play: Analysis of prehospital IV fluid therapy by computer simulation," *Ann. Emerg. Med.*, vol. 19, no. 2, pp. 163–168, Feb. 1990, doi: 10.1016/S0196-0644(05)81802-5.

[25]   F. Lewis, "Prehospital Intravenous Fluid Therapy: Physiologic Computer Modelling," *J. Trauma Inj. Infect. Crit. Care*, vol. 26, no. 9, pp. 804–811, Sep. 1986.

[26]   R. Bighamian, A. T. Reisner, and J.-O. Hahn, "A Lumped-Parameter Subject-Specific Model of Blood Volume Response to Fluid Infusion," *Front. Physiol.*, vol. 7, Aug. 2016, doi: 10.3389/fphys.2016.00390.

[27]   P. A. Ioannou and J. Sun, *Robust Adaptive Control*. Mineola, New York: Dover Publications, Inc, 2012.

[28]   N. S. Nise, *Control Systems Engineering*, Eighth edition. Hoboken, NJ: Wiley, 2019.

[29]   H. K. Khalil, *Nonlinear Control*, Global ed. Boston: Pearson, 2015.

[30]   J.-J. E. Slotine and W. Li, *Applied Nonlinear Control*. Englewood Cliffs, N.J: Prentice Hall, 1991.

[31]   L. S. Costanzo, *Physiology*, Sixth edition. Philadelphia, PA: Elsevier, 2018.

[32]   R. Bighamian, M. Kinsky, G. Kramer, and J.-O. Hahn, "In-human subject-specific evaluation of a control-theoretic plasma volume regulation model," *Comput. Biol. Med.*, vol. 91, pp. 96–102, Dec. 2017, doi: 10.1016/j.compbiomed.2017.10.006.

[33]   C. R. Monnard, B. Fellay, I. Scerri, and E. K. Grasser, "Substantial Inter-Subject Variability in Blood Pressure Responses to Glucose in a Healthy, Non-obese Population," *Front. Physiol.*, vol. 8, Jul. 2017, doi: 10.3389/fphys.2017.00507.

[34]   A. C. Guyton, *Arterial pressure and hypertension*. Philadelphia: Saunders, 1980.

[35]   A. C. Guyton, H. J. Granger, and A. E. Taylor, "Interstitial fluid pressure," *Physiol. Rev.*, vol. 51, no. 3, pp. 527–563, Jul. 1971, doi: 10.1152/physrev.1971.51.3.527.

[36]   J. G. O'Brien, S. A. Chennubhotla, and R. V. Chennubhotal, "Treatment of Edema," *Am. Fam. Physician*, vol. 71, no. 11, pp. 2111–2117, Jun. 2005.

[37]   J.-L. Vincent, "Understanding cardiac output," *Crit. Care Lond. Engl.*, vol. 12, no. 4, p. 174, 2008, doi: 10.1186/cc6975.

[38]   D. A. Beard and E. O. Feigl, "Understanding Guyton's venous return curves," *Am. J. Physiol. Heart Circ. Physiol.*, vol. 301, no. 3, pp. H629-633, Sep. 2011, doi: 10.1152/ajpheart.00228.2011.

[39]   J. E. Hall and A. C. Guyton, *Textbook of Medical Physiology*. 2016.

[40]   A. D. Rafie *et al.*, "Hypotensive Resuscitation of Multiple Hemorrhages Using Crystalloid And Colloids," *Shock*, vol. 22, no. 3, pp. 262–269, Sep. 2004, doi: 10.1097/01.shk.0000135255.59817.8c.

[41]   N. R. Marques *et al.*, "Automated closed-loop resuscitation of multiple hemorrhages: a comparison between fuzzy logic and decision table controllers in a sheep model," *Disaster Mil. Med.*, vol. 3, no. 1, p. 1, Jan. 2017, doi: 10.1186/s40696-016-0029-0.

[42]   S. Vaid *et al.*, "Normotensive and hypotensive closed-loop resuscitation using 3.0% NaCl to treat multiple hemorrhages in sheep*," *Crit. Care Med.*, vol. 34, no. 4, pp. 1185–1192, Apr. 2006, doi: 10.1097/01.CCM.0000207341.78696.3A.

[43]   S. Henschen, M. W. Busse, S. Zisowsky, and B. Panning, "Determination of plasma volume and total blood volume using indocyanine green: a short review," *J. Med.*, vol. 24, no. 1, pp. 10–27, 1993.

[44] L. Ljung, *System Identification: Theory for the User*. Pearson Education, 1998.

[45] M. Niedźwiecki, *Identification of Time-Varying Processes*. Chichester ; New York: Wiley, 2000.

[46] K. J. Keesman, *System Identification: An Introduction*. Springer London, 2011.

[47] K. J. Åström and B. Wittenmark, *Adaptive Control*, 2nd ed., Dover ed. Mineola, N.Y: Dover Publications, 2008.

[48] K. S. Naren and A. M. Annaswamy, *Stable Adaptive Systems*. 2012.

[49] A. C. Guyton, "The Relationship of Cardiac Output and Arterial Pressure Control.," *Circulation*, vol. 64, no. 6, pp. 1079–1088, Dec. 1981, doi: 10.1161/01.CIR.64.6.1079.

[50] X. Jin, R. Bighamian, and J.-O. Hahn, "Development and In Silico Evaluation of a Model-Based Closed-Loop Fluid Resuscitation Control Algorithm," *IEEE Trans. Biomed. Eng.*, vol. 66, no. 7, pp. 1905–1914, Jul. 2019, doi: 10.1109/TBME.2018.2880927.

[51] R. G. Hahn, "Volume Kinetics for Infusion Fluids," *Anesthesiol. J. Am. Soc. Anesthesiol.*, vol. 113, no. 2, pp. 470–481, Aug. 2010, doi: 10.1097/ALN.0b013e3181dcd88f.

[52] J.-J. E. Slotine and W. Li, "Composite adaptive control of robot manipulators," *Automatica*, vol. 25, no. 4, pp. 509–519, Jul. 1989, doi: 10.1016/0005-1098(89)90094-0.

[53] C. Bergek, J. H. Zdolsek, and R. G. Hahn, "Accuracy of noninvasive haemoglobin measurement by pulse oximetry depends on the type of infusion fluid," *Eur. J. Anaesthesiol.*, vol. 29, no. 12, pp. 586–592, Dec. 2012, doi: 10.1097/EJA.0b013e3283592733.

[54] L. Ljung and S. Gunnarsson, "Adaptation and tracking in system identification—A survey," *Automatica*, vol. 26, no. 1, pp. 7–21, Jan. 1990, doi: 10.1016/0005-1098(90)90154-A.

[55] J. R. Varvel, D. L. Donoho, and S. L. Shafer, "Measuring the predictive performance of computer-controlled infusion pumps," *J. Pharmacokinet. Biopharm.*, vol. 20, no. 1, pp. 63–94, Feb. 1992, doi: 10.1007/bf01143186.